Biomaterial inks and bioinks for fabricating 3D biomimetic lung tissue: a delicate balancing act between biocompatibility and mechanical printability

Karamchand, Leshern; Makeiff, Darren; Gao, Yongfeng; Azyat, Khalid; Serpe, Michael J.; Kulka, Marianna

Publisher's version / Version de l'éditeur:
https://doi.org/10.1016/j.bprint.2022.e00255
Bioprinting, 29, C, 2022-11-16

Bioprinting 29 (2023) e00255

Contents lists available at ScienceDirect

Bioprinting

journal homepage: www.sciencedirect.com/journal/bioprinting

Biomaterial inks and bioinks for fabricating 3D biomimetic lung tissue: A delicate balancing act between biocompatibility and mechanical printability

Leshern Karamchand [a], Darren Makeiff [a], Yongfeng Gao [b], Khalid Azyat [a], Michael J. Serpe [b], Marianna Kulka [a,*]

[a] National Research Council Canada, Nanotechnology Research Centre, 11421, Saskatchewan Drive NW, Edmonton, AB, T6G 2M9, Canada
[b] University of Alberta, Department of Chemistry, 11227, Saskatchewan Dr NW, Edmonton, AB, T6G 2N4, Canada

ARTICLE INFO

Keywords:
Biomimetic
Biomaterial ink
Bioink
3D lung tissue
Microgel/nanogel
Supramolecular gel

ABSTRACT

Three dimensional (3D) bioprinting has rapidly emerged as a major fabrication tool in the bioengineering of tissue constructs. 3D bioprinting enables the precise deposition of nano, micro and macroscale tissue components to produce tissue models that more closely mimic the unique and complex architecture of their corresponding *in vivo* tissues. Despite the vast potential of 3D bioprinting to revolutionize tissue engineering, few biomimetic models of lung tissue have been reported in the literature to date, which is largely owed to the lung's highly complex branching tubular network that permits gaseous transport and exchange with its inextricably integrated blood supply system. This review focuses on the repertoire of natural and synthetic polymers that have been employed thus far to fabricate hydrogel-based tissue constructs of various regions of the lung airway network. The applicability of novel biocompatible materials, such as micro- and nanogels and self-assembling low molecular weight gelators, to the fabrication of lung tissue constructs are also discussed. The essential criteria that these biomaterial inks must fulfill from both biological and engineering perspectives, including biomimicry, biocompatibility, biodegradability and rheology, are emphasized within the context of current 3D bioprinting technology.

1. Introduction

Three-dimensional (3D) bioprinting has evolved at the interface of three independent disciplines, namely, biofabrication, tissue engineering (TE)/regenerative medicine (RM), and additive manufacturing [1–3]. The collective technological advances in these respective fields have enabled the production of physiologically functional tissues through the positioning of cells and biocompatible materials with high spatial resolution in three dimensions. Importantly, the physiological function of any tissue is inextricably connected to the unique architecture of its cellular constituents and extracellular matrix (ECM), as well as the composition of the interstitial fluid which contains a milieu of biochemical signals and growth factors. By controlling the deposition of tissue components spanning the nano- and microscales, 3D bioprinting can produce biomimetic tissue models that accurately replicate the unique and complex architecture of their corresponding *in vivo* tissues [4]. In 3D bioprinting, the fabrication of biomimetic tissue models is achieved through the stratification of a 3D computer-aided design (CAD) model into 2D cross-sectional slices, which are then transmitted to a 3D bioprinter that sequentially assembles the 3D tissue construct in a layer-by-layer fashion using bioprintable materials, either *bioinks* or *biomaterial inks*, via one of several bioprinting techniques (Fig. 1). A *bioink* is essentially "a formulation of cells suitable for processing by an automated biofabrication technology that may also contain biologically active components and biomaterials," whereas a *biomaterial ink* is "a formulation that includes biologically active components or molecules, but does not contain any cells, which however can be subsequently seeded with cells after printing" [5]. It should be emphasized that bioinks contain cells as a mandatory component of the printable formulation, which may be in the form of single cells, coated cells and cell aggregates, or in combination with materials such as microcarriers, microgels, physical hydrogels or hydrogel precursors [5]. Hence, the biofabrication of a 3D tissue construct may be performed either directly (pre-seeding/bottom-up method) using bioinks, or indirectly

* Corresponding author.
E-mail address: Marianna.Kulka@nrc-cnrc.gc.ca (M. Kulka).

https://doi.org/10.1016/j.bprint.2022.e00255
Received 1 June 2022; Received in revised form 5 November 2022; Accepted 9 November 2022
Available online 16 November 2022

(post-seeding/top-down method) using biomaterial inks – the former involves simultaneous printing of a cell-laden bioink, whereas the latter involves initial printing of the construct exclusively with the biomaterial ink, which is co-cultured with the desired cell type(s) post-fabrication (Fig. 1) [6].

Irrespective of the bioprinting approach taken, bioinks and biomaterial inks play a vital role in supporting cells during and/or after printing, in addition to serving as a scaffold to facilitate the attachment of cells, and potentially promote them to revert to their native cellular morphology after printing, which would be especially beneficial to tissue-resident cell types. In essence, bioinks and biomaterial inks are multi-functional materials that must possess specific physicochemical properties to, (i) ensure their compatibility with the selected 3D bioprinting technique to facilitate reproducible high-resolution printing, (ii) maintain a high degree of biocompatibility with cells without eliciting undesirable activation of cell functions, (iii) completely polymerize and sustain structural integrity of the construct after printing, (iv) be perfusable and ventilatable, and (v) promote nutrient diffusion and tissue maturation during the post-printing culture phase, including cellular activities such as adhesion, differentiation, migration and proliferation. The architecture of the bioink scaffold is especially crucial with respect to accurately mimicking a specific tissue type as this ultimately influences its mechanical properties [7], and in turn, affects biological processes [8] as well as the distribution of oxygen, carbon dioxide, nutrients and waste across the tissue construct [9,10].

Although the lung is considered a solid organ from a surgical perspective, from a tissue engineering standpoint, the lung is viewed as a complex, branching matrix of tubes. Because of this complexity, few 3D bioprinted lung tissue models have been attempted, particularly that of the distal lung where gaseous exchange occurs. Gaseous exchange regions consist of intricate tissue architectures with single-cell resolution while simultaneously exhibiting sufficient elasticity to permit repetitive expansion and contraction cycles, without incurring damage or impairing the efficacy of gaseous exchange. Additionally, lung tissue is a dynamic system whereby immune cells sample the lung lumen and monitor for microbial infection. Several early attempts were made to fabricate *in vitro* lung tissues [11–13], but a functionally perfusable and ventilatable 3D-bioprinted alveolar tissue model was only realized in 2019 [14]. This is largely due to the fact that most of the currently available bioinks do not meet all the requirements for the fabrication of the complex lung tissue scaffold, i.e., strength, elasticity, promotion of cell adhesion and biodegradability. It is noteworthy that, while various 3D bioprinting technologies have developed rapidly since the late 1980s, the innovation and advancement of bioink technologies to complement these 3D bioprinting modalities have been comparatively slower and only gained substantial momentum in recent years [15]. However, recent innovation in bioink technology has expanded the repertoire of bioprintable materials beyond pre-existing natural polymer hydrogels, such as alginate, gelatin and hyaluronic acid, to include a range of synthetic polymer hydrogels, and advanced materials, such as micro- and nano-structured hydrogels. This review focuses on the essential physicochemical criteria that bioinks must fulfill in order to facilitate reproducible fabrication of functional, biomimetic 3D lung tissue architecture, as well as the recent advances in bioink technology that can enable the fabrication of both normal and disease models of the lung.

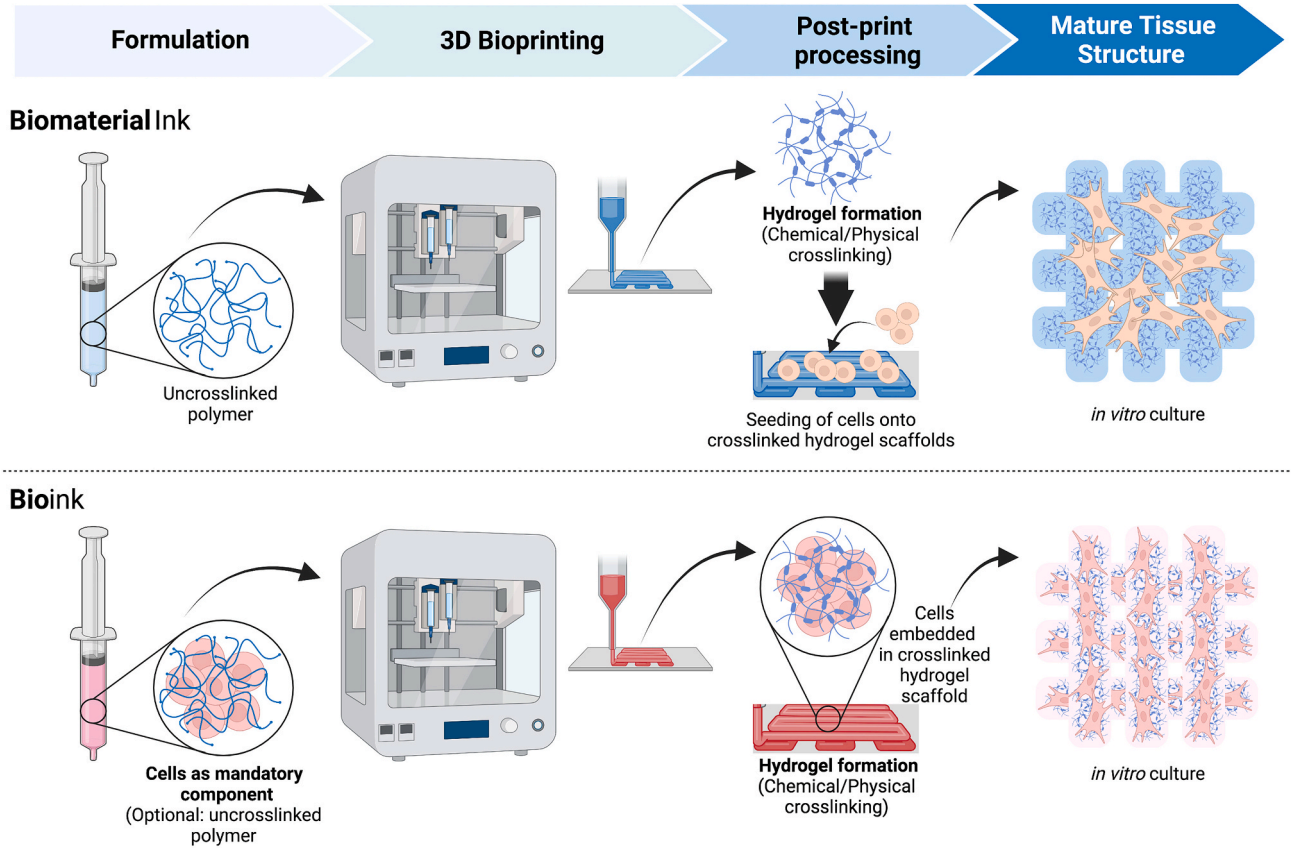

Fig. 1. Comparison of the post-seeding/top-down bioprinting approach using biomaterial inks and the pre-seeding/bottom-up bioprinting approach using bioinks. (Created with BioRender.com).

2. Overview of lung architecture

The human lung consists of 23 generations of bifurcating air passages, which originate at the trachea with a diameter of 1.8 cm and progressively decreases in diameter to 500 μm at the respiratory bronchioles (Table 1) [16]. There are two general zones within the lung: the conducting and respiratory zones. The conducting zone of the lung consists of the trachea, main bronchi and terminal bronchioles, which are not involved in gas exchange (Fig. 2). The trachea and main bronchi are composed of cartilage rings and cartilage plates, respectively, that are surrounded by smooth muscle and connective tissue to prevent their collapse – an anatomical feature that distinguishes them from the smaller airways. The lumen of the conducting airways are lined with pseudostratified epithelium (25–40 μm in thickness), which comprise only a single layer of cells attached directly to the basement membrane, however, the variable positioning of the nuclei of individual epithelial cells relative to the basement membrane is reminiscent of cellular stratification in histological sections. The cellular constituents of pseudostratified epithelium include goblet, submucosal mucous, submucosal serous, surface serous, brush, and club (Clara) cells, which collectively function to secrete mucous and remove trapped particles via ciliary action (Fig. 2) [16].

The epithelium of the respiratory bronchioles are predominantly composed of cuboidal-shaped club cells with fewer ciliated subpopulations, including pulmonary neuroendocrine and goblet cells (Fig. 3). The respiratory bronchioles terminate at the pulmonary acini that consist of numerous, single alveoli, and alveolar sacs, which are approximately 200 μm in diameter (Fig. 2). The respiratory bronchioles, alveoli and alveolar sacs collectively constitute the respiratory zone. The wall of a single alveolus consists of only a single layer of epithelial cells that are in direct contact with the underlying endothelial cells of the alveolar capillaries. Hence, the septum that separates two adjacent alveolar spaces consists of only four cell layers, ranging in thickness from 0.2 to 4 μm [18,19]. The human lung is estimated to contain 480 million alveoli in total, which occupy ~65% of the lung surface area [20]. The alveolar epithelium consists of alveolar type 1 (AT1) and alveolar type 2 (AT2) cells (Fig. 3). AT1 cells facilitate gas exchange with the capillary endothelial cells, while AT2 cells secrete surfactant to reduce surface tension at the air-liquid interface within the small volume of the alveolar space [21]. In addition, alveolar epithelial cells, specifically the surfactant-producing AT2 cells, play a significant role in controlling the growth of the pathogen, *Mycobacterium tuberculosis (M.tb)*, as demonstrated by a murine lung-on-chip model of *M.tb* infection [22]. AT1 cells constitute more than 90% of the lung's surface area despite being a minor cellular population of the lung parenchyma (<11%), whereas AT2 cells are a more abundant cellular population of the lung parenchyma (12–16%) yet only constitute around 7% of the lung's surface area [23]. The alveolar capillaries wrap around each alveolar space, and confine the flow of erythrocytes (red blood cells) in single file around the alveolar spaces. This architecture maximizes the release of carbon dioxide from deoxygenated erythrocytes into the alveolar space, and the simultaneous absorption of oxygen from the alveolar space into the erythrocytes. The organization and maintenance of the intricate pulmonary architecture is the function of the pulmonary extracellular matrix (ECM), which will be discussed in further detail in the *Biomimicry* section.

As the airway transitions from the conducting zone to the respiratory bronchioles and terminates in the alveolar sacs, the luminal diameter becomes progressively narrower (Table 1) with a concomitant decrease in thickness and change in cellular composition of the epithelial lining (Fig. 3). The lung airway architecture is further

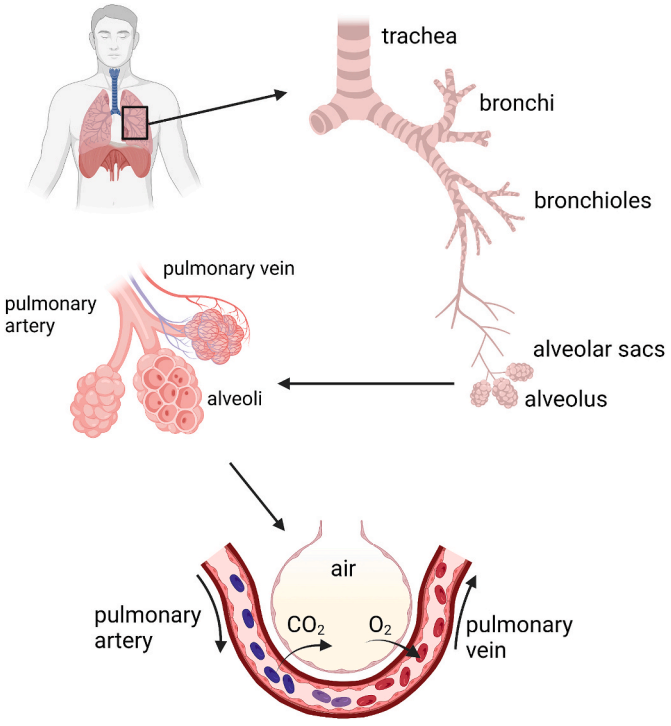

Fig. 2. Schematic diagram depicting the bifurcating nature of the pulmonary airway system that starts at the trachea and terminates in individual alveoli, the sites at which gaseous exchange occurs. (Created with BioRender.com).

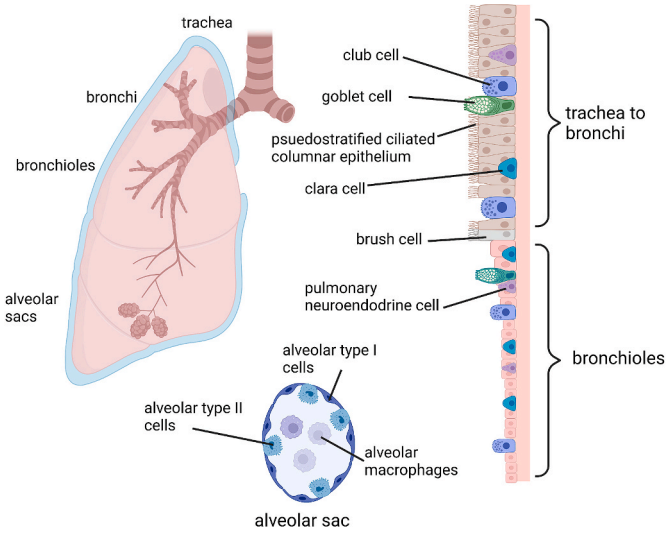

Fig. 3. Schematic diagram depicting the cellular structure of the epithelial linings of the trachea, bronchi, bronchioles and alveolar sacs that should be ideally recapitulated by 3D bioprinted structures. (Created with BioRender.com).

Table 1
Typical dimensions of various human lung airway structures [17].

	Zone Type	Diameter (mm)	Length (mm)
Trachea	Conducting	18.0	120
Bronchi	Conducting	12.2–8.3	48–8
Bronchioles	Conducting/Respiratory	4.5–0.5	13–1
Alveolar sacs	Respiratory	0.4	0.5
Alveolus	Respiratory	0.1–0.2	–

complicated by its highly branched nature, and inextricable integration with a dual vascular system, i.e., the respiratory zone airways are supplied with deoxygenated blood transported via the pulmonary veins, while the thicker and more metabolically active conducting zone airways are supplied with oxygenated blood transported via the bronchial arteries (Fig. 2). Hence, the sheer complexity of the lung airway architecture, which encompasses size scales ranging from centimeters to microns, and multiple cell types that are functionally integrated with a dynamic ECM and vasculature, poses a significant challenge to the fabrication of biomimetic lung tissue by 3D bioprinting [24,25].

A wide array of 3D bioprinting methods now exist for the fabrication of tissue models, including extrusion-based bioprinting, inkjet-based bioprinting, fused-deposition modelling, laser-assisted forward transfer bioprinting, and stereolithography. The reader is referred to other excellent reviews in the literature that discuss and compare these bioprinting techniques in greater detail [26–28]. However, neither of these bioprinting techniques alone are capable of fabricating a contiguous airway network across a broad scale range, from the trachea through to the terminal alveolar sacs, with the single-cell resolution required to reproduce functional gas exchange surfaces with the blood capillary network. Nonetheless, the potential exists to leverage individual bioprinting techniques, within the scope of their respective strengths and limitations, to fabricate different sections of the lung airway architecture, as summarized in Table 2.

Extrusion-based bioprinting is the most commonly employed method in tissue engineering due to its versatility, ability to process the broadest range of bioink viscosities, and ability to print tissues at clinically relevant throughput and ease, with which strata consisting of different types of biomaterials, cells, signaling molecules and growth factors can be fabricated [29]. The moderate resolution (>100 μm) of extrusion-based bioprinting and fused-deposition modeling makes these techniques amenable to the fabrication of larger airway structures such as the trachea and bronchi. Artificial cartilage rings and plates can be fabricated from thermo-responsive biomaterials, such as polycaprolactone, using fused-deposition modeling to support the tracheal and bronchial constructs, followed by the deposition of hydrogel-encapsulated cells around the artificial cartilage supports to form hollow tubular structures [30–32]. Inkjet-based deposition has a higher printing resolution (10–50 μm), does not subject cells to sheer stress-induced damage like extrusion-based bioprinting, and is therefore more amenable to the printing of the complex airway epithelium, which is only a single cell layer thick. Laser-assisted forward transfer, which has an intermediate printing resolution (50–300 μm) can be leveraged to fabricate smaller airway structures such as the bronchioles, alveolar sacs and, potentially, alveoli. Stereolithography has the capability of rapidly fabricating complex, high-resolution scaffolds from photo-crosslinkable biomaterials, and is therefore amenable to replicating the complex 3D architectures of alveolar sacs, alveoli and their integrated capillary networks [14]. Recently, Copploe et al. generated computational models of eight generations of the neonatal tracheobronchial tree comprising the conducting zone airways, which were then fabricated into 3D models using a photopolymer (Somos® WaterShed SC 11122) via stereolithography [33]. While this model lacked the finer airway structures (bronchioles, alveolar sacs and alveoli), the authors demonstrated the immense potential of computational modeling and stereolithography in fabricating a contiguous and integrated human lung airway tree.

3. Biomaterial inks and bioinks

3.1. Essential properties of biomaterial inks and bioinks for lung tissue fabrication

Polymeric biomaterials that can be crosslinked into hydrogels post-fabrication are especially amenable to the biofabrication of soft tissues due to their (i) ability to encapsulate cells in a hydrated environment, (ii) biodegradability, and (iii) chemical and mechanical properties that mimic the native extracellular matrices (ECM) of various tissue types [35,36]. In the case of bioinks, the cellular component(s) of the formulation place more stringent constraints on the processing conditions that the bioink can be subjected to during and after printing as compared to biomaterial inks that are devoid of cells. Therefore, bioinks and biomaterial inks must satisfy several criteria, including biomimcry, biocompatibility, biodegradability, and rheology, in order to produce functional tissues while being simultaneously compatible with the chosen bioprinting method [37].

3.1.1. Biomimicry

The crucial function of any biomaterial ink is to emulate the ECM of *in vivo* tissue so as to facilitate natural cellular adhesion and morphology. The ECM was long believed to serve merely as a support platform for cells, but is now considered to be a vital and highly dynamic mediator in healthy and diseased tissues. The pulmonary ECM not only provides structural integrity, but also binds to specific adhesion receptors on cells, activating intracellular signaling cascades that influence cellular behaviors such as adhesion, proliferation, migration, epithelial-to-mesenchymal transition, apoptosis for maintaining homeostasis, and the production and secretion of mediators. Furthermore, the ECM serves as a reservoir of growth factors and cytokines [38–40].

The pulmonary cellular constituents are organized into various tissues by the pulmonary ECM, which are classified into two main structural types: (i) basement membranes and (ii) interstitial matrices. Basement membranes are thin sheets of glycoproteins that line the basal side of epithelia and endothelia, and surround other cell types such as fat, muscle and peripheral nerve cells. Interstitial matrices form loose, fibril-like mesh networks that interconnect structural cell types that form the lung parenchyma, and therefore maintain the 3D structure and

Table 2
Comparison of 3D bioprinting techniques and potential applications to fabrication of different lung airway structures [26,27,34].

	Extrusion-based deposition	Fused-deposition modelling	Inkjet-based deposition	Laser-assisted forward transfer	Stereolithography
Bioink/Biomaterial ink Viscosity (mPa·s)	$<6 \times 10^7$	N/A (Thermo-responsive melting)	3–12	1–300	No restriction
Maximum cell density	No restriction	No restriction	$< 10^6$ cells/mL	$< 10^8$ cells/mL	No restriction
Resolution	Moderate (>100 μm)	Moderate (>100 μm)	High (10–50 μm)	High to medium (50–300 μm)	High (<100 μm)
Fabrication scale	Modeling of 10 cm scale constructs	Modeling of 10 cm scale constructs	Modeling of cm scale constructs	Modeling of mm scale constructs	Modeling of 10 cm scale constructs
Potential airway fabrication application	Trachea, bronchi	Trachea, bronchi	Trachea, bronchi, Bronchioles	Bronchioles, Alveolar sacs, Alveoli	Alveolar sacs, Alveoli, Blood Capillaries

biomechanical properties of the lung [39,40]. The lung undergoes repeated cycles of stretch and relaxation, typically greater than 14,000 times per day, which the pulmonary ECM accommodates while still maintaining the structural integrity of the lung 3D architecture. In humans, the pulmonary ECM consists of several protein components. Fibrillar collagens (types I, II, III, V and XI) confer high tensile strength but low elasticity. Elastins confer high elasticity but low tensile strength. Laminins and collagen type IV constitute the basement membranes in the majority of the alveolar sacs and airways, while fibronectin and proteoglycans maintain lung cell polarity and survival [38,40]. The fibrillar collagens contribute to the overall 3D architecture of the lung, whereas the large elastic fibers confer compliance and elastic recoil to the lung [41,42]. Elastic fibers are composed of an inner core comprising cross-linked elastin, while the periphery consists of microfibrils [43]. The microfibrils are composed of the large glycoproteins, fibrillin-1, 2 and 3 [44], in addition to the microfibril-associated glycoproteins, fibulins, elastin microfibril interface-located proteins (EMILINs), elastin-crosslinking lysyl oxidases (LOXs), and microfibrillar-associated protein 4 (MFAP4) [43,45]. Proteoglycans (PGs) consists of a protein core covalently linked to sulfated polysaccharides or glycosaminoglycans (GAGs). Due to their high polysaccharide content, PGs are hydrophilic, which enables hydrogel formation (an important property for biomaterial inks as discussed in sections 3.1.4 and 4.1), and contributes overall to the viscoelastic properties of the lung. The main cellular producers of the ECM proteins are fibroblasts and myofibroblasts, and also include airway epithelial cells and airway smooth muscle (ASM). Fibroblasts are key cell mediators that regulate the homeostasis of ECM proteins by coordinating the secretion of matrix metalloproteases (MMPs) and their inhibitors, as well as integrating signals from the ECM [46,47]. Hence, the above mentioned cells that regulate ECM homeostasis are an essential cellular subset that should be incorporated into biomimetic 3D lung tissue models.

The *matrisome* constitutes the proteomic profile of the ECM of a specific tissue type [48]. Booth et al. recently characterized the matrisome of normal and idiopathic pulmonary fibrotic (IPF) lung tissue by liquid chromatography/tandem mass spectrometry [38]. Of the 94 distinct proteins that were identified in the normal lung matrisome, 61 were core ECM proteins (glycoproteins, collagens, and proteoglycans), while 33 were ECM-related proteins, which underscores the phenomenal complexity of the lung ECM. The IPF lung matrisome expressed a similar proteomic profile of 85 proteins (64 core ECM as well as 21 other ECM-related proteins), however, the most profound difference between the normal and IPF matrisomes was observed in the changes in relative abundance of specific proteins. For example, the IPF matrisome was enriched with collagen types III and VI, periostin, matrix G1a protein, nephronectin, ECM-related proteins such as, glycosaminoglycans, and transforming growth factor beta (TGF-β) binding protein 1, while being relatively deficient in alveolar basement membrane proteins such as, laminin α-3, β-3, and γ-2 chains, relative to the normal lung ECM. Booth et al. further observed significant phenotypic differences in primary human lung fibroblasts that were cultured in decellularized normal and IPF ECM slices. Fibroblasts grown in normal lung ECM exhibited low alpha smooth muscle actin (α-SMA) production, whereas fibroblasts grown in IPF lung ECM demonstrated significantly elevated production of α-SMA, which is consistent with myofibroblast differentiation [49]. Collectively, the data highlighted the profound role that the ECM plays in lung pathology and modulating cellular phenotypes. Hence, careful consideration of the ECM composition is necessary when attempting to fabricate biomimetic analogs of both normal and disease models of human lung tissue. Naturally-derived hydrogel polymers, such as collagen, fibronectin, and laminin, which contain cell-adhesive peptide sequences that promote proliferation, migration and sustain cell viability, can individually emulate specific supportive features of the native ECM more effectively than unmodified synthetic polymers. Conversely, synthetic polymers can be chemically functionalized with bioactive functional groups, such as the arginine-glycine-aspartate (RGD) peptide sequence derived from the ECM protein fibronectin to stimulate cell adhesion [50].

3.1.2. Biocompatibility

A biocompatible bioink/biomaterial ink is required to maintain high cell viability, support cell growth and proliferation, and preserve the cell population's healthy, characteristic phenotype in the formulation [51–53]. Importantly, the bioink/biomaterial ink should not elicit cytotoxicity, premature stem cell differentiation, or host inflammatory responses if the biofabricated tissue is implanted within the body. Additionally, the bioink/biomaterial ink should not dampen or alter the normal responses of any immunological cells encapsulated within the tissue construct. Therefore, the mandatory, initial step in lung tissue engineering is to identify the degree of biocompatibility of a biomaterial with the different constituent cell types. Aside from the biomaterial ink itself, the encapsulated cells may experience a range of stresses from the bioprinting process that can affect their viability, phenotype, behavior and function. These stresses include, (i) physical mixing to create a homogeneous formulation of the cellular and biomaterial components, (ii) shear forces encountered during extrusion of the bioink from narrow gauge nozzles (typically a few hundred microns in diameter), and (iii) exposure to UV light, photoinitiators, and rapid changes in pH, temperature and ionic strength that are required to crosslink and facilitate gelation of the bioink. It is therefore essential to determine biocompatibility both during printing [54] and post-printing [51]. Dubbin et al. assessed cell viability at different flow rates during extrusion-based bioprinting, as well as during ionic- and photo-crosslinking of six different bioinks [54], in which they observed that higher flow rates during extrusion-based bioprinting correlated with lower cell viability (between 5 and 11% cell death), while photo-crosslinking elicited significantly higher cell death than ionic-crosslinking (calcium chloride, 10 mM). Notably, cell death was observed to be higher at the edges of the hydrogel constructs than at the center in both types of crosslinking. This has direct implications on the bioprinting of lung airway epithelial linings that are only one-cell layer thick and exposed to air, and therefore prone to desiccation especially during the extended print times required to fabricate tubular airway structures on the scale of tens of cm. Bedell et al. developed a standardized, high-throughput method for assessing the biocompatibility of different biomaterial ink formulations on printed human mesenchymal stem cells (hMSCs) [51]. This approach involved droplet printing of hMSCs encapsulated in various biomaterial inks at two different cell densities in 96-well microtiter plates, which enables high-throughput and multiplexed screening of cytotoxicity, cell proliferation and phenotype (cell surface receptor expression) several days after printing.

Bioprinted lung tissue constructs can be implanted *in vivo* to recapitulate functional tissue or as an *in vitro* model to study biochemical responses and drug efficacy. Lung tissue constructs that are intended for *in vivo* implantation should ideally be immunologically inert and evade or dampen host immune responses, although this is often difficult to achieve given that many biomaterials activate resident immune cells. One of the most obvious immune reactions to implanted foreign constructs is the foreign body reaction (FBR) in which mast cells, macrophages, neutrophils, fibroblasts and lymphocytes initiate a localized inflammatory response resulting in the formation of a fibrous capsule or granuloma surrounding the foreign material [55]. The FBR can also result in the formation of foreign body giant cells which are essentially monocyte-derived macrophages that have undergone a highly controlled process of cell-cell fusion under the control of integrins, CD44, CD47 mannose receptors and chemokines such as CCL2 [55].

Each process of foreign body cell formation is likely unique to the biomaterial and composition of the implant. Alginate activates resident monocytes and macrophages to produce cytokines such as tumor necrosis factor (TNF), which induces mast cells to release histamine and initiates recruitment of lymphocytes [56–58], although much of these responses may be mediated by contaminants found in alginate preparations rather than the alginate itself. The biodegradation products of gelatin, collagen and fibronectin, activate macrophages through pattern recognition receptors (PRRs) initiating innate immune responses and localized inflammation [55], although there is some evidence to suggest that this could be in part due to the cross-species incapability of the protein constituents [59]. Hyaluronic acid activates cells via CD44 and hyaluronic acid hydrogels activate foreign body reactions in four to eight weeks after transplantation [60,61]. In some individuals, polyethylene glycol (PEG) elicits a relatively potent immune response characterized by the production of anti-PEG IgM and IgG and generation of memory T cells [62]. A recent Japanese study suggests that as many as 20% of individuals that have an underlying immune response to PEG, which renders the use of PEG difficult to apply broadly [63]. Polyglycolic acid (PGA) can initiate xenogeneic inflammatory responses [64]. Even the surgical procedure required to implant a constructed tissue itself elicits a localized immune response, which can recruit lymphocytes and granulocytes to the region, thereby initiating further immune cascades [65]. Therefore, these materials must be used with caution when bioprinting lung tissue for eventual transplantation. These materials must also be carefully evaluated if these bioprinted constructs are to be used as immunocompetent model systems for drug testing as the matrix materials themselves may activate background inflammatory responses.

Tissue constructs that are used as *in vitro* models for research purposes should be functional and have a multifaceted immune cell repertoire. Although most tissue constructs contain the structural cells that define the tissue (i.e., epithelial cells, fibroblasts, endothelial cells), they lack the tissue-specific immune cells that facilitate and regulate localized tissue responses to therapeutics. Since macrophages, dendritic cells, mast cells and neutrophils are essential components of lung tissue, the lung has been considered an important immune organ [66]. Although these types of immune cells regulate much of the biophysical processes in the lung, both in constitutive and pathogenic states, they are difficult to recapitulate in biomaterial constructs due to their fragility and short half-life [67]. Without these important immune cells in a biomaterial construct it is difficult to extrapolate observed responses to healthy human lungs.

Another important consideration in avoiding inadvertent inflammatory responses is ensuring that the bioink/biomaterial ink is devoid of endotoxin, such as the highly immunogenic lipopolysaccharide (LPS), which is shed from the surface of bacteria [68]. This necessitates aseptic (sterile) handling of the bioink/biomaterial ink during production and throughout the biofabrication process, and is especially crucial for animal-derived biopolymers such as decellularized extracellular matrix (dECM).

3.1.3. Biodegradability

The biomaterial ink components of the fabricated lung tissue construct must be able to provide mechanical support post-printing, yet be able to undergo gradual biodegradation in order to permit tissue remodeling and maturation without degrading during printing, which is especially crucial when synthetic hydrogel polymers are used. Therefore, the rate of decomposition of the biomaterial scaffold should be tuned to match the rate of tissue maturation to assist cells such as fibroblasts to replace the synthetic polymers with native lung ECM components [69]. The hydrogel byproducts should ideally be monomers that are water soluble, non-toxic, non-immunogenic, and can undergo biotransformation in the liver and/or renal excretion. In addition, the hydrogel byproducts should not damage the cellular components of the tissue construct and/or the surrounding tissues if implanted *in vivo*. The rate of decomposition is ultimately dependent on the specific biomaterial ink employed, and the mechanisms of hydrogel biodegradation include hydrolytic, ion exchange, and enzymatic reactions [70]. Hydrolytic and ion exchange-based reactions typically occur in a bulk manner, thus leading to a constant rate of biodegradation. In contrast, the rate of enzymatic reactions is dependent on both the number of cleavage sites present within the polymer and the enzyme concentration, and therefore offers a greater degree of control. Control over the decomposition rate of hydrogel polymers can be achieved by one of several approaches. The first involves optimization of the cell density/polymer ratio. Since cells are a source of matrix proteases, lower cell densities and higher polymer concentrations can result in prolonged biodegradation times, although this will reduce the efficacy of tissue regeneration. The second approach involves the covalent modification of hydrogel polymers with peptides bearing enzymatic cleavage sites that enable site-specific and controllable decomposition, while the third approach involves modulating the degree of cross-linking. Increasing the polymer concentration, cross-linker concentration, and exposure time to the cross-linker can achieve a higher degree of cross-linking and thus lower decomposition rates. From an engineering perspective, biodegradable biomaterial inks can also be leveraged in the fabrication of the highly-branched tubular airway network of the lung. This can conceivably be achieved by bioprinting interconnected cylindrical and micro-spherical structures from biodegradable biomaterial inks that serve as scaffolds for the attachment of epithelial cells and other pulmonary cell types. After a period of tissue maturation, the biodegradable biomaterial ink can be dissolved to leave behind an interconnected network of hollow tubes and cysts, essentially serving a sacrificial role.

3.1.4. Rheological properties

Ideal biomaterial inks and bioinks must also satisfy several rheological criteria in order to be printable, which can be considered as *"the ability of a material, when subjected to a certain set of printing conditions, to be printed in a way which results in printing outcomes which are desirable for a given application"* [71]. The majority of biomimetic lung tissue models to date have been fabricated primarily from hydrogel-based biomaterial inks and bioinks via extrusion-based 3D bioprinting in a bottom-up approach, which have specific rheological requirements as discussed in greater detail in other comprehensive reviews [72,73]. Briefly, hydrogel-based biomaterial inks and bioinks are typically deposited via piston- or pneumatic-based extrusion systems due to their lower viscosity ($<10^7$ mPa s) [74] as opposed to screw-driven extrusion systems that are better suited to extruding higher viscosity materials (up to 10^4 Pa s) [4]. Shear-thinning is the most favorable type of time-independent non-Newtonian fluid behavior for extrusion bioprinting, whereby increasing shear rates result in a concomitant decrease in viscosity of the biomaterial ink/bioink, thus permitting its extrusion, followed by recovery and shape retention. Hydrogels that possess shear-thinning properties are especially beneficial to the extrusion of cell-laden bioinks as their viscosities decrease significantly during extrusion, thus limiting the exposure of cells to excessive shear forces that can induce cell membrane damage and lead to reduced cell viability after printing. The shear forces that cells are subjected to during extrusion can be further reduced by formulating bioinks from partially cross-linked hydrogels or pregel solutions as these fluids exhibit significantly lower viscosities than completely gelated hydrogels. Pregels exhibit shear-thinning properties as the polymers involved in the molecular networks undergo disentanglement

and reorientation along the direction of the shear flow. This is possible due to physical cross-linking between the polymers based on ionic or hydrogen bonds, or hydrophobic interactions. These hydrogel cross-linking mechanisms are discussed in further detail in section 3.1.5 *Hydrogels*. Alternatively, hydrogels from jammed suspensions, which are densely packed microgels or nanogels that form colloidal-like suspensions, can be used to limit the exposure of cells to excessive shear forces during extrusion, as discussed in further detail in section 3.4.4 *Micro- and Nanogels*.

3.1.5. Hydrogels

Hydrogels are insoluble 3D polymeric networks that have the ability to swell and absorb large amounts of water without disintegration [75,76]. Hydrogels can be composed up to 99% water content by weight, which is comparable to biological tissues [35,77–79]. The hydrophilicity of hydrogels is owed to the presence of functional groups within the polymer chains that can form hydrogen bonds such as, hydroxyl (-OH), carboxyl (-COOH), amide (–CONH–), primary amide (-$CONH_2$) and urea (–NHCONH–) groups [80]. Additional features that make hydrogels attractive for tissue engineering applications are the ability to mimic the ECM, tunable characteristics for efficient and homogeneous seeding of various cells, as well as the porous structure to confine cells to specific compartments and allow for the transfer of different nutrients required for cell viability and differentiation (i.e., adsorption of proteins, cell migration, proliferation, and vascularization of newly formed tissues in the scaffolds) [29,81,82].

The structural integrity of a hydrogel is maintained by crosslinks between the individual polymer chains, which allows it to remain insoluble despite its inherently high water content. The degree and type of cross-linking during synthesis controls the porosity, pore size, elasticity, viscosity, degree of swelling and shape fidelity of the hydrogel [83]. Importantly, the cross-linking of hydrogels for lung tissue fabrication is a fine-balancing act – a low degree of crosslinking yields hydrogels that are sufficiently viscous with the ability to flow freely but at the expense of stability, conversely a high degree of cross-linking improves stability. However, excessive cross-linking produces hydrogels that are too stiff with poor flow characteristics for extrusion-based bioprinting and poor elastic recoil to accommodate repetitive ventilation cycles, which can also affect cell development and differentiation [84–88]. Generally, cross-linking mechanisms are categorized as either physical or chemical, and the method may be dependent on the candidate bioink under consideration for 3D bioprinting. Importantly, the majority of hydrogel-based bioinks/biomaterial inks actually contain hydrogel precursors that can be cross-linked into hydrogels post-printing, whereas only a few examples involve the pre-formation of a gel prior to printing such as, synthetic peptide-polymer hybrids [89] and spider silk protein-based hydrogels [90].

Physical cross-links. The types of physical interactions that drive gelation include, self-assembly/aggregation, coacervate gelation and ionotropic gelation. Physical cross-linking encompasses a range of weak, noncovalent interactions such as ionic bonding, hydrogen bonding, π-π stacking, van der Waals forces, metal-ligand (coordinative), and hydrophobic forces [84]. The cumulative effect of these weak interactions promotes entanglement of the polymer chains driving self-assembly/aggregation, thus resulting in gelation. Coacervate gelation is the result of a combination of attractive forces between biopolymers, but is mostly driven by repulsive, hydrophobic forces between the biopolymers and solvent. Ionotropic gelation is driven by the complexation of a cation (e.g. bivalent Ca^{2+} ions) by several anionic moieties contained within the polymer chains resulting in strong reticulation nodes. Although physical cross-links are reversible, they are sufficient to render the hydrogel insoluble in aqueous media. The reversibility of physically cross-linked hydrogels allows the bioink to be extruded in a pre-cross-linked state, however, this poses a challenge to the structural integrity of 3D tissue models that are cultured for extended periods of time. Ionic cross-linked hydrogels, such as Ca^{2+} cross-linked alginate, are especially vulnerable to dissolution in *in vitro* culture or *in vivo* due to the diffusion of Ca^{2+} ions from the hydrogel into the culture medium or surrounding extracellular fluid. A key feature of physically cross-linked hydrogels is that they do not require additional cross-linking agents (e.g. photoinitiator, coupling agent) to achieve gelation, with the exception of ions in the case of ionotropic gelation. This obviates the need for further processing steps to remove any excess cross-linking agents that could adversely affect the viability of cells in the tissue model.

Chemical cross-links. Chemical cross-linking involves the formation of permanent covalent bonds between adjacent polymer chains, and can be achieved through various polymerization methods (chain growth, addition, condensation and photo-based) and small molecule-mediated cross-linking [84]. Hydrogel bioinks that are chemically cross-linked exhibit higher mechanical strength than physically cross-linked hydrogels. However, a caveat of chemical cross-linking is that fully cross-linked hydrogel bioinks form irreversibly, have poor flow characteristics, and are therefore difficult to extrude through high gauge (narrow diameter) print nozzles. One solution to this problem involves the initial extrusion of a partially-cross-linked bioink followed by a post-printing secondary cross-linking step to enhance the structural integrity of the hydrogel tissue. This can be achieved by developing a hybrid bioink that is partially cross-linked by physical methods and subsequently stabilized by a chemical method such as photopolymerization. Photopolymerization is a covalent chemical cross-linking strategy that typically involves the rapid cross-linking of acrylate-functionalized polymer chains by free-radicals that are generated upon activation of a photoinitiator (Fig. 7) by UV light (365 nm or 405 nm) [91,92].

3.2. Scaffold-based biomaterial inks

Biomaterial inks and bioinks can be broadly categorized as either scaffold-based or scaffold-free, and is based on whether the cells that compose a tissue construct are printed with or without a supporting scaffold [93,94]. The primary function of scaffold-based bioinks is to mimic the biochemical characteristics and microenvironment of the lung extracellular matrix (ECM), however it is indeed challenging for one specific bioink to holistically mimic the function and properties of the lung ECM. These scaffold-based formulations include; (i) hydrogel polymers that emulate the cross-linked network of the ECM while simultaneously encapsulating large volumes of cells in a hydrated environment, and (ii) decellularized extracellular matrices (dECM) that are derived by the removal of cellular components from harvested animal tissues. Scaffold-based biomaterial inks can be either naturally- or synthetically-derived. Naturally-derived bioinks have typically been preferred due to their superior ability to mimic the biochemical properties of the lung ECM with fewer cytotoxic effects. However, synthetic bioinks have the advantages of greater mechanical strength and chemical tunability to make 3D bioprinted lung tissues conducive to the mechanical stresses of repeated stretch and relaxation cycles associated with breathing. Commonly used natural and synthetic polymers that form hydrogels and are suitable for co-formulation with dECM biomaterial inks to fabricate lung tissues, cell encapsulation and 3D bioprinting are hereafter summarized in Section 3.3 and Table 3.

Table 3
Comparison of dECM, Natural and Synthetic Polymer Hydrogels Used to Fabricate Lung Tissue Models.

Biomaterial	Polymer Type	Gelation Mechanism	Bioprinting Method	Function*	Lung Tissue/Cell Types Printed
Human lung dECM/ Porcine lung dECM// Matrigel	Decellularized tissue/organs	Thermo-responsive (Gelation at 37 °C)	Extrusion-based deposition	Support, Functional	1. Human lung dECM hydrogel scaffold (allogenic lung fibroblasts) [97], 2. Porcine lung dECM hydrogel (bone marrow-derived human mesenchymal stem cells (hMSCs), rat MSCs) [99,101], 3. Vascularized airway-on-a-chip model (Porcine tracheal mucosa dECM, polycaprolactone, human dermal microvascular endothelial cells, human lung fibroblasts, primary human tracheal epithelial cells) [100], 4. Murine lung explants (Matrigel) [102], 5. *In vitro* air-blood barrier alveolar model (Matrigel, EA.hy926 human endothelial cells, A549 human AT2 epithelial cells) [103], 6. Alveolar epithelial viral infection model (Matrigel, gelatin, alginate, A549 human AT2 epithelial cells) [105], 7. Bronchial airway model (Alginate-reinforced human lung dECM, murine and human lung epithelial cells (MLE12 and A549), murine brain endothelial cells (bEND.3), primary human bronchial epithelial cells (HBECs), primary lung smooth muscle cells (HLSMCs)) [111].
Alginate	Natural, Polysaccharide	Ionic crosslinking	Extrusion-based deposition	Structural, Sacrificial	1. Trachea airway model (Alginate, polycaprolactone, Alveolar epithelial cells, chondrocytes, chondrogenic-differentiated bone marrow-derived MSCs) [30–32], 2. Alveolar epithelial viral infection model (Alginate, Matrigel, gelatin, A549 human AT2 epithelial cells) [105], 3. Alveolar epithelial viral infection model (Alginate, Collagen type I, gelatin, human primary fibroblasts, THP-1 monocytes, A549 human AT2 epithelial cells) [107], 4. Bronchial airway model (Alginate-reinforced human lung dECM, murine and human lung epithelial cells (MLE12 and A549), murine brain endothelial cells (bEND.3), primary human bronchial epithelial cells (HBECs), primary lung smooth muscle cells (HLSMCs)) [111].
Hyaluronic Acid	Natural, Polysaccharide	Photocrosslinking (requires chemical modification)	Extrusion-based deposition	Functional, Structural	1. Human MSCs (MSC to AT2 epithelial cell transition) [114].
Collagen/Gelatin	Decellularized tissue/organs, Protein	Thermo-responsive (Gelation at room temperature)	Extrusion-based deposition	Functional, Structural, Sacrificial	1. Triple-layered human alveolar model (Rat tail collagen type I, polyvinvylpyrrolidone, MRC-5 human lung fibroblasts, EA.hy296 endothelial cells, A549 AT2 epithelial cells) [104], 2. Alveolar epithelial viral infection model (Alginate, Matrigel, gelatin, A549 human AT2 epithelial cells) [105], 3. Alveolar epithelial viral infection model (Alginate, Collagen type I, gelatin, human primary fibroblasts, THP-1 monocytes, A549 human AT2 epithelial cells) [107].
Silk Fibroin	Natural, Protein	Organic solvent-mediated gelation (methanol)	Extrusion-based deposition	Structural	1. Lung epithelial model (Silk fibroin, TEMPO-oxidized bacterial cellulose nanofibrils, lung epithelial stem cells) [125].
Pluronic F-127	Synthetic	Thermo-responsive (Gelation at > 10 °C)	Extrusion-based deposition	Sacrificial	1. Tubular lung airways (Pluronic F127, porcine lung dECM, MSCs) [101].
Polycaprolactone	Synthetic	Thermo-responsive melting	Thermal extrusion-based deposition	Structural	1. Trachea airway model (Alginate, polycaprolactone, Alveolar epithelial cells, chondrocytes, chondrogenic-differentiated bone marrow-derived MSCs) [30–32], 2. Vascularized airway-on-a-chip model (Porcine tracheal mucosa dECM, polycaprolactone, human dermal microvascular endothelial cells, human lung fibroblasts, primary human tracheal epithelial cells) [100].
PEG (PEO)/PEGdiPDA	Synthetic	Photocrosslinking (requires chemical modification)	Stereolithography (SLATE)	Structural/ Sacrificial	1. Alveolar sac (Endothelial cells, AT2 epithelial cells) [14,127].

* Biomaterial inks sub-categorized according to their function, i.e., support, sacrificial, structural and functional biomaterial inks [5]. **Support biomaterial inks** serve as artificial ECMs, and depending on the biomaterial's properties, physical or chemical gelation may occur resulting in a solid structure after extrusion, which may or may not occur reversibly [70]. **Sacrificial biomaterial inks** are temporary materials that can be selectively dissolved to create internal channels or pores within tissue constructs to better facilitate gaseous and nutrient exchange. **Structural biomaterial inks** are composed of materials that provide mechanical integrity to

tissue constructs. **Functional biomaterial inks** provide various cues, e.g., biochemical, electrical or mechanical, to influence cellular behavior during *in vitro* culture of the tissue constructs.

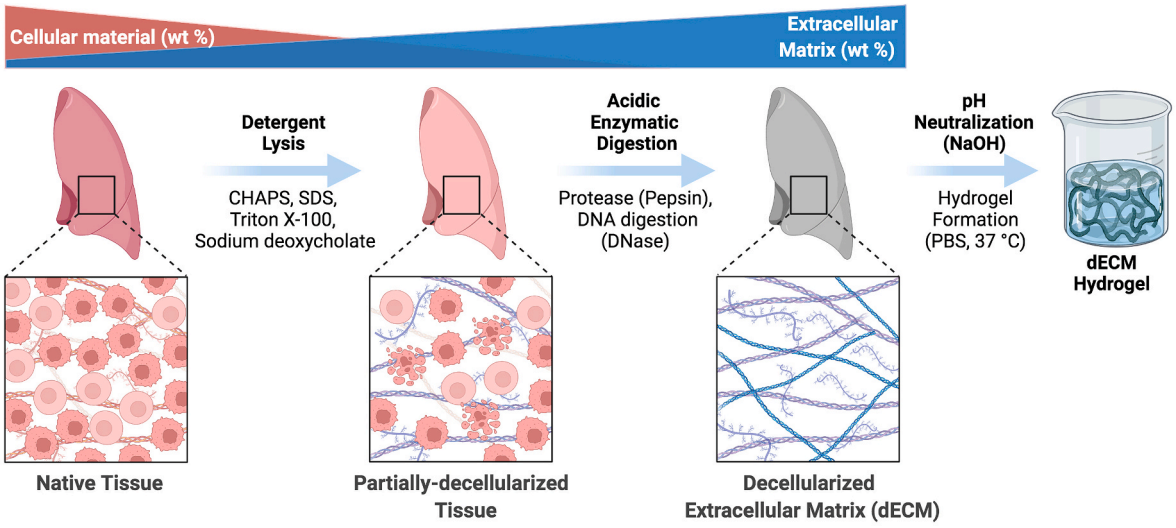

Fig. 4. General procedure involved in the production of decellularized extracellular matrix (dECM) hydrogels from harvested organ tissues for 3D bioprinting applications. (Created with BioRender.com).

3.3. dECM, natural and synthetic hydrogel polymers used in lung tissue fabrication

3.3.1. Decellularized extracellular matrices (dECM)

The process of producing decellularized extracellular matrices (dECM) involves the removal of ~98% of cells from living tissues thus leaving behind the ECM (Fig. 4) [95]. Due to their biological origin, dECM-based bioinks exhibit the highest cell viability and lowest cytotoxicity of all biopolymer-based bioinks [96]. The generation of ECM from intact tissue is achieved using a combination of detergents (e.g., CHAPS, sodium dodecyl sulfate (SDS), sodium deoxycholate, Triton X-100), followed by gentle proteolytic cleavage, typically with pepsin in acidified solution (acetic or hydrochloric acid), and DNA degradation with DNases for up to 72 h. Thereafter, the dECM suspension undergoes pH neutralization with NaOH, which also deactivates pepsin, and an adjustment to physiological osmolarity, typically with PBS, at 37 °C, which spontaneously yields a hydrogel [97,98]. Rosmark et al. prepared dECM lung scaffolds from donor human lung tissue and characterized changes to the lung matrisome before and after repopulating the acellular scaffolds with allogenic lung fibroblasts by LC-MS/MS analysis [97]. The decellularization process was found to efficiently remove loosely attached ECM associated matrisome proteins, thus increasing the initial relative proportion of core-matrisome proteins (collagens, ECM glycoproteins and proteoglycans) from 66% to 96%. The reintroduction of allogenic lung fibroblasts into the scaffolds resulted in an initial increase in the relative proportion of ECM affiliated proteins, ECM regulators and secreted factors, which indicated that the fibroblasts had replaced the matrisome proteins that were depleted during the decellularization process. After nine days of culture, the relative proportion of core matrisome proteins started to increase. Ultimately, the lung fibroblasts remodeled the matrisome of the dECM scaffold to resemble the composition to native tissue sections, which the authors found to be superior to the ECM composition secreted by fibroblasts cultured in standard monolayer cultures. This observation emphasizes the dynamic and interdependent relationship between fibroblasts and the ECM, whereby the fibroblasts secrete various ECM components, which in turn interact with and activate signaling pathways within the fibroblasts and influence their cell behavior as well as that of other cells within the tissue matrix.

Initial attempts at developing lung dECM hydrogels for tissue engineering were derived from porcine lung tissue [99,100]. Pouliot et al. extracted dECM from porcine lung tissue and subsequently converted the lung dECM into hydrogels [99]. The authors then encapsulated bone marrow-derived human mesenchymal stem cells (hMSCs) within the porcine lung dECM hydrogels, which exhibited enhanced attachment and viability compared to hMSCs encapsulated within a commercial hydrogel composed of only collagen. In addition, *in vivo* experiments involving rat MSCs that were encapsulated in the porcine dECM pre-gel solution and delivered to an emphysema rat model, significantly increased cell retention in the lung over a 24 h period. Expression levels of the Sox2 and Oct4 genes, which are responsible for maintaining the pluripotency and stem-like nature of MSCs, increased significantly at day 3 after encapsulation, but then returned to control levels at day 7, suggesting that the MSCs retained their original phenotype. The porcine lung dECM hydrogel showed little to no gelation activity until the temperature of the material exceeded 32 °C, however the pre-gel solution self-assembled into a hydrogel within 3 min upon reaching 37 °C, which is the typical gelation profile of dECM biomaterial inks.

More recently, Falcones et al. developed a biomaterial ink with tunable stiffness based on porcine lung dECM hydrogels, which they then used to 3D bioprint and culture rat lung-resident MSCs without the need for additional chemical or physical crosslinking of the hydrogels (gelation was achieved by incubation at 37 °C for 30 min) [101]. The stiffness was varied by changing concentration of the ECM powder in the hydrogel preparation. Specifically, the high-concentration (20 mg/mL) lung dECM (HC-L-dECM) pregels formed hydrogels with microscale mechanics, which were closest to that of lung parenchyma tissue. After gelation, G′ and G″ of the HC-L-dECM hydrogels were 4.91 Pa and 1.85 Pa, respectively, which signified good printability (ease of extrusion) of the HC-L-dECM and their ability to retain their shape after printing. The MSCs exhibited high viability after 7 days of culture, and good Z-distribution throughout the construct signifying that the cells did not settle after 3D bioprinting and gelation. Moreover, the morphology of the MSCs cultured in the 3D scaffolds were markedly different with respect to MSCs grown in conventional 2D monolayers. Furthermore, cell contraction assays demonstrated the existence of viable MSC–matrix interactions within the 3D bioprinted scaffolds. The adhesion capacity and length of the focal adhesions formed by the MSCs in the 3D scaffolds

were also significantly higher compared to MSCs cultured in 2D monolayers. Additionally, MSCs within the 3D scaffolds exhibited a greater than 20-fold increase in the expression of the CXCR4 receptor compared to MSCs cultured in 2D monolayers. In an *in vitro* model of acute respiratory distress syndrome, the MSCs exhibited significantly lower secretion of pro-inflammatory mediators (IL-6) when cultured within the 3D scaffolds. Hence, this study provided a viable approach to culturing lung MSCs in 3D hydrogel scaffolds, which could potentially provide greater insight into their immunomodulatory properties, and thus their therapeutic potential with respect to lung tissue repair. Recently, Fang et al. reported that endogenous pulmonary mesenchymal stem cells (pMSCs) contributed to repair of the airway epithelium following injury in a murine model, whereby the pMSCs migrated into the airway epithelium layer, and sequentially differentiated transitionally to epithelial stem cells, such as neuroendocrine cells, and finally to newly differentiated Club cells, ciliated cells, and goblet cells [102]. Hence, the inclusion of pMSCs in 3D bioprinted lung tissue can confer self-regeneration capability to the fabricated tissue allowing it to replace the delicate cells of the pulmonary epithelium that are highly susceptible to damage when subjected to sheer stress during extrusion-based bioprinting.

In a separate study, Park et al. developed a functional airway-on-a-chip model by encapsulating human dermal endothelial cells (ECs) and lung fibroblasts within a lung tissue dECM hydrogel derived from porcine tracheal mucosa (tmdECM), which were then 3D bioprinted within a polycaprolactone frame [100]. After 3D bioprinting, the tmdECM gradually facilitated endothelial re-orientation, which led to the formation of a lumen and vascular network. Endothelial cells encapsulated in tmdECM expressed significantly higher levels of various angiogenic genes (PECAM, VE-cadherin, VEGF and VEGF-R) compared to ECs encapsulated in a collagen type I only hydrogel. Thereafter, the authors assembled a fully-differentiated *in vitro* airway model comprising primary human tracheal epithelial cells with the 3D bioprinted vascular platform to emulate the interaction between alveolar epithelial cells and endothelial cells that comprise the alveolar capillaries. The vascularized airway-on-a-chip model also effectively reproduced respiratory symptoms of asthmatic airway inflammation and allergen-induced asthma exacerbation, which are physiologically relevant.

Another commonly used ECM hydrogel in 3D bioprinting is the commercially available Matrigel™, which is derived from the basement matrix extracted from Engelbreth-Holm-Swalm mouse sarcomas, and has been in use for more than 40 years. Horvath et al. 3D bioprinted an *in vitro* air-blood barrier using a combination of Matrigel, human EA.hy926 (endothelial) cells and human A549 AT2 epithelial cells in order to replicate the alveolar ultrastructure [103]. This process first involved the extrusion of a thin layer of Matrigel onto a porous membrane, followed by a subsequent layer of EA.hy926 endothelial cells directly on top of the Matrigel layer (Day 0). On day two, a second thin layer of Matrigel was extruded directly onto the EA.hy926 endothelial cells, followed immediately thereafter by a layer of A549 alveolar epithelial cells. The printing order is summarized as follows: *Matrigel → EA.hy926 → Matrigel → A549*. The 3D bioprinted double-cell layered alveolar construct was cultured for three further days and evaluated. This approach enabled automated and reproducible fabrication of thinner and more homogeneous cell layers compared to manually seeding, and more closely mimicked the *in vivo* alveolar septal wall that is only 4 cell layers thick. In a subsequent study, Ng et al. [104] used a similar approach to Horvath et al. [103], with some modifications, to 3D bioprint a triple-layered human alveolar lung model. This triple-layered model comprised of MRC-5 human lung fibroblasts (basal/lower layer), EA.hy926 endothelial cells (middle layer) and A549 AT2 epithelial cells (upper layer), which were extruded as bioink formulations with 2.5% w/v polyvinvylpyrrolidone (PVP) at different cell densities. The authors also used collagen type I (rat tail) instead of Matrigel as the biomaterial ink to bond the different cells layers to each other in the following printing order: *Collagen → MRC-5 → EA.hy926 → Collagen → A549*. Each cell type in the triple-layer model exhibited sustained cell proliferation rates up to seven days post-printing, which were not significantly different from that of control, non-printed cells for each cell type. The triple-layer alveolar lung models were initially cultured at the liquid-liquid interface (LLI, submerged) for three days, and then transferred to the air-liquid interface (ALI) for either four, seven, or eleven days. In general, the alveolar tissue models exhibited >96% viability over a total period of 14 days using the hybrid LLI-ALI culture conditions. Immunocytochemical analysis of the alveolar lung models confirmed the expression of Pro-SPC (AT-2), pan cytokeratin (epithelial lung cells), and CD31 (endothelial cells) biomarkers, suggesting that the cell types retained their phenotypes after 3D bioprinting. Notably, the ALI culture condition lead to an increased expression of pro-SPC (AT-2) and pan-cytokeratin (epithelial) biomarkers at day seven, as compared to the LLI culture condition. Lastly, the overall thickness of the human alveolar lung models in this study was determined to be 8–10 μm using confocal microscopy, which is approximately 2–2.5 times thicker than the human alveolar septal wall *in vivo*.

Berg et al. recently demonstrated the 3D bioprinting of a human alveolar lung tissue model using a hybrid biomaterial ink formulation comprising sodium alginate (2% w/v; crosslinker): gelatin (3% w/v): Matrigel (20% w/v), which efficiently supported infection with Influenza A virus [105]. Sodium alginate is a poly-anionic linear polysaccharide derived from brown algae that undergoes rapid cross-linking when exposed to a calcium ionic solution through sodium-calcium ion exchange to form a hydrogel [106]. Gelatin and Matrigel undergo thermal gelation (solidification) at 20 °C and 37 °C, respectively. Hence, calcium-mediated crosslinking of alginate permits the initial gelation of the bioink, while gelatin maintains gelation during the printing process at 20 °C. Thereafter, gelatin dissolves, acting as a 'sacrificial' biomaterial ink protein, during the post-printing incubation phase of the tissue model at 37 °C, at which point the gelation of Matrigel takes over and maintains the structural integrity of the tissue model during tissue culture. Rheometric analyses of the crosslinked alginate-gelatin-Matrigel hydrogel revealed that the G′:G′′ ratio was highest at a Matrigel concentration of 20% (w/v), but then decreased when the Matrigel concentration was increased to 50% (w/v). Similarly, the shear viscosity of the gelatin-Matrigel-alginate pre-gel remained low at 20% (w/v) Matrigel, but then increased dramatically when the Matrigel concentration was increased to 50% (w/v). The authors selected A549 cells for bioprinting their lung tissue models with the alginate-gelatin-Matrigel biomaterial ink instead of human primary AT2 epithelial cells, which can only be cultured for a limited period of time before transdifferentiating into AT1 epithelial cells. The distribution of A549 cells and Influenza A viral particles throughout the 3D bioprinted scaffolds was most uniform at a Matrigel concentration of 20% (w/v). Additionally, the cell viability of A549 cells, and the Influenza A viral titer were highest in hydrogel scaffolds with 20% (w/v) Matrigel. A clustered pattern of infection of A549 cells with Influenza A virus was observed in the 3D bioprinted scaffolds, but not in 2D monolayer cultures of A549 cells, which also observed in the lung *in vivo*. The scaffolds also supported the release of pro-inflammatory interferon by the infected cells in response to the virus. The major drawback of this lung tissue model is that it consisted of only AT2 epithelial (A549) cells. Hence, in their follow-up study, Berg et al. [107] reported more complex 3D bioprinted lung tissue models from biomaterial inks comprising alginate (3% w/v), gelatin (3% w/v), Collagen type I (0.5 mg/mL) instead of Matrigel, and the three cellular constituents including human primary fibroblasts, THP-1 monocytes, and A549 cells. Viral inhibition assays with the 3D bioprinted lung model supported the restricted replication of Influenza A virus with an antiviral agent in a dose-dependent manner. Furthermore, the 3D bioprinted lung models generated an immune response (release of pro-inflammatory cytokines IL-1β and IL-8) when challenged with a combination of bacterial toxins, LPS and ATP. This study marked a significant stride in the development of *in vitro* human lung tissue

models towards studying the replication dynamics of airborne pathogens and the immune response to such pathogens.

An advantage of using Matrigel to generate 3D tissue models as opposed to collagen alone, is that it recapitulates the features of natural ECMs due to its complex composition [108]. However, the use of Matrigel in 3D tissue engineering applications is severely limited by its ill-defined and variable composition, and as a result, inconsistent biochemical properties between different batches, and even within the same batch, which can lead to poor cell reseeding efficacy [109]. Matrigel is also susceptible to degradation by matrix metalloproteases secreted by cells that are reseeded into the ECM hydrogel [95], which is especially problematic if the bioprinted tissues are implanted *in vivo*. Additionally, the gelation of Matrigel cannot be precisely controlled, which occurs over a wide temperature range (22–37 °C) and timescale (minutes to hours), and therefore cannot be reliably processed via extrusion 3D bioprinting [109]. Furthermore, the use of ECM hydrogels derived from porcine or other animal tissues for xenotransplantation poses the risk of transmission of pathogens, such as porcine endogenous retroviruses (PERVs) [110] as well as the elicitation of immune responses by the human immune system towards antigenic moieties contained within the animal-derived dECM [109].

To circumvent the above mentioned drawbacks of animal-derived dECMs, De Hilster et al. recently generated lung dECM hydrogels from donor lung tissue and compared the biomechanical properties of the lung dECM hydrogels to that of the native whole lung tissue by rheometry [98]. The lung dECM hydrogel exhibited a significantly lower Young's modulus (lower stiffness or resistance to deformation under load) than that of the native whole lung tissue. Concomitantly, the lung dECM hydrogel exhibited significantly higher stress relaxation than the native whole lung tissue, i.e., the lung dECM hydrogel relaxed completely after compression during the 200 s observation phase, whereas the native lung tissue did not. These observations were attributed to the absence of cells in the dECM hydrogel, which would otherwise be involved in cross-links with the ECM components, and therefore confer greater stiffness to the ECM.

More recently, De Santis et al. developed a hybrid biomaterial ink system comprising human lung dECM reinforced with sodium alginate (rECM) [111]. Importantly, not all dECM solutions can spontaneously form hydrogels, or they suffer from slow gelation kinetics. Since sodium alginate is rapidly crosslinked with a $CaCl_2$ solution (50 mM) within 5 min, the authors circumvented the inherently poor gelation properties of dECM-based biomaterial inks by combining sodium alginate (4% w/v) with lung dECM (10 mg/mL) in a 1:1 ratio (2% w/v alginate: 5 mg/mL dECM final concentrations). The inclusion of sodium alginate also served to confer a support structure to the dECM biomaterial ink, which enabled the formation of more complex scaffold geometries using extrusion 3D bioprinting. Rheometric analysis confirmed that the rECM exhibited better sheer thinning behavior ($G' > G''$) compared to alginate alone, which is essential for the pre-gel solution to be extruded during 3D bioprinting, and for the hydrogel to retain its shape after gelation. Furthermore, the rECM exhibited increased mechanical stability under shear stress compared to alginate-only hydrogels at the same weight percentage. The rECM bioink was significantly better at resisting cell sedimentation than alginate only after 3D bioprinting and gelation, and significantly enhanced the viability of several cell types; i.e., murine and human lung epithelial cells (MLE12 and A549, respectively), murine brain endothelial cells (bEND.3), and primary human bronchial epithelial cells (HBECs). The 3D bioprinted rECM constructs suppressed the foreign body response, supported angiogenesis and recipient-derived *de novo* blood vessel formation in a murine model of transplant immune-suppression. The rECM bioink also enabled the 3D bioprinting of segmental bronchi (~4 mm in diameter) composed of an inner layer of HBECs and two sequential outer layers of primary human lung smooth muscle cells (HLSMCs). The 3D bioprinted bronchial airways remained viable and patent (ability to maintain airflow for breathing) for up to one month in ALI culture with further evidence of differentiation into mature epithelial cell types as found in native human airways. Hence, the hybrid rECM biomaterial ink meets the requirements for printability by extrusion 3D bioprinting, mechanical stability, biocompatibility, biomimicry and the ability to support diverse cell types that are required for angiogenesis and formation of complex, functional airway tissues for potential transplantation.

3.3.2. Alginate

Alginate is a linear polysaccharide block copolymer consisting of β-D-mannuronic acid (M) and α-L-guluronic acid (G) monosaccharide residues (Fig. 5A) that is produced by brown algae and some species of bacteria. The polysaccharide sequence is irregular due to the presence of regions of consecutive G-blocks, consecutive M-blocks, or alternating M-blocks and G-blocks. The molecular weight of alginate can range between 10 and 600 kDa, but is typically between 50 and 180 kDa. Alginate is an attractive hydrogel polymer for bioprinting due to its

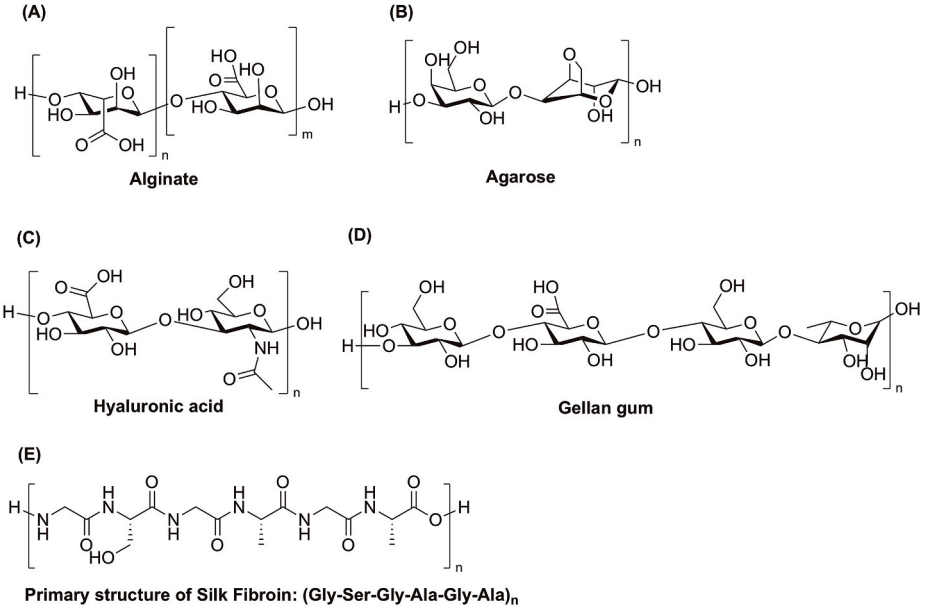

Fig. 5. Chemical structures of natural biopolymers used in the formulation of biomaterial inks and bioinks: (A) alginate, (B) agarose, (C) hyaluronic acid, (D) gellan gum, and (E) silk fibroin. Alginate, agarose and gellan gum are polysaccharides that undergo ionotropic gelation with calcium ions, whereas hyaluronic acid is a glycosaminoglycan that requires additional chemical modification, such as with methacrylate groups, to facilitate covalent photo-crosslinking. Silk fibroin is a polypeptide that undergoes self-assembly into anti-parallel β-sheet secondary structures.

structural similarities to natural ECMs, excellent biocompatibility, viscosity, and the ease of gelation that takes place at room temperature [112]. Alginate is commonly used in 3D bioprinting applications as aqueous sols (~3% w/v), and while it possesses acceptable viscosity for extrusion, it lacks shear thinning behavior. After extrusion, ionic cross-linking of the alginate scaffold is initiated by immersion in aqueous solutions containing divalent metal ions such as calcium, strontium, barium, or zinc. Ionic interactions (physical complexation) of the metal ions with the carboxyl and hydroxyl groups of the guluronic acid residues within the alginate polymer chains results in the formation of stable hydrogels. The resulting chelate complex has been described by the so-called 'egg box model' [113]. The stiffness of alginate hydrogels are easily adjusted by selecting the appropriate molecular weight of alginate and concentration of divalent metal ion used for cross-linking. Ionotropic gelation of alginate with calcium ions is a fully biocompatible process (at least up to Ca^{2+} concentrations of 100 mM). Hence, alginate-based bioinks are currently among the most commonly used in bioprinting. Since alginate does not contain cell-binding moieties, such as the RGD peptide sequence of fibronectin, it does not permit cell adhesion which is necessary for cell viability, thereby leading to "anoikis" (apoptosis due to the absence of cell adhesion). Adhesion is also necessary to promote cell differentiation, and in the absence of stimuli to differentiate, cells tend to change phenotype and fail to respond normally. This drawback may be overcome by the co-formulation of alginate with gelatin (2% w/v)/Matrigel (20% w/v) [105], gelatin (3% w/v)/collagen type I (0.5 mg/mL) [107], or lung dECM (5 mg/mL) [111] that promote cell adhesion, migration and differentiation for lung tissue models, as discussed previously in the section on dECM biomaterial inks.

Recently, several groups fabricated biomimetic tracheal grafts using a co-formulation of polycaprolactone, a thermo-responsive polymer that exhibits similar strength to tracheal cartilage, and alginate (3% w/v) hydrogels encapsulating respiratory epithelial cells, chondrocytes and/or chondrogenic-differentiated bone marrow-derived mesenchymal stem cells, which were subsequently transplanted into the trachea of New Zealand White rabbits [30–32]. In each of these studies, histological analysis of the transplants demonstrated successful integration of the tracheal graft and regeneration of the respiratory epithelium, blood vessels, and cartilage tissue.

3.3.3. Hyaluronic acid

Hyaluronic acid (HA, hyaluronan) is a linear glycosaminoglycan composed of β-1,4-linked D-glucuronic acid (β-1,3) and N-acetyl-D-glucosamine disaccharide residues (molecular weight range of 10 to 10,000 kDa, Fig. 5C). HA is a major component of the healthy lung ECM, which confers elasticity and hydrophilicity to tissues and plays an important role in the structure of the alveolar surface stabilizing the surfactant proteins. Sala et al. recently demonstrated that low and medium molecular weight HA stimulated the differentiation of MSCs into AT2 epithelial cells and promoted their expression and secretion of surfactant proteins, mimicking the physiological alveolar microenvironment [114]. Hence, the inclusion of HA as an ECM component in the fabrication of alveolar sac structures is crucial to the optimal physiological function of the AT2 cells.

While HA has excellent biocompatibility, and biodegradability by the hyaluronidase enzyme [115], the foremost limitation with bioprinting unmodified HA is the low stability and stiffness of the bioprinted scaffolds due to the high water solubility of HA. Therefore, the formation of HA-based hydrogels requires high HA concentrations (>2 mg/mL) and/or chemical modification of its saccharide residues. Previously reported HA chemical modifications that permit the spontaneous formation of hydrogels without requiring the addition of initiators include, disulfide addition, haloacetate, hydrazide, aldehyde, tyramine (enzymatic), and click reactions [115]. The derivatization of HA with methacrylate groups allows the HA chains to undergo photo-crosslinking with UV light. Hence, the degree of photo-crosslinking can be controlled by the level of methacrylation introduced into the HA formulation and the length of time during which the HA scaffolds are exposed to UV light after extrusion.

3.3.4. Collagen/gelatin

Collagens are a family of fibrillar proteins that have a characteristic triple helical structure (polyproline-II type) with a molecular range of 100–300 kDa. The primary structure is composed of repeating tripeptide (Gly-X-Y) motifs, where X and Y are mainly proline, hydroxyproline, lysine, hydroxylysine and alanine. Proline and hydroxyproline play a pivotal role in stabilizing the super-helical tertiary structure through steric hindrance. Importantly, the polypeptide chains also contain RGD (arginyl-glycyl-aspartyl) motifs that enable cell adhesion via integrin-RGD binding interactions. As discussed earlier, collagen is a major constituent of the ECM of human tissues, including the lung, and is involved in numerous physiological interactions. Due to their exceptional biocompatibility, low cytotoxicity and biodegradability, collagens, particularly collagen type I, are commonly used to fabricate biomimetic tissue scaffolds. Due to the highly-structured super-helical tertiary structure of collagens, enzymatic (pepsin) or acidic treatment after extraction from animal tissue (e.g. rat tail) are required to yield homogeneous pregel solutions (from 1.5 mg/mL) that are suitable for extrusion-based 3D bioprinting [116]. However, 3D bioprinted scaffolds based on collagen alone lack sufficient structural integrity, and therefore have to be co-formulated with other biopolymers, such as alginate, to increase the viscosity and enhance shape retention after gelation, as reported by Berg et al. in their fabrication of a multi-cell type human lung model [107].

Heat denaturation of collagen disrupts its primary, secondary and tertiary (triple helical) structures resulting in a random coiled protein conformation known as gelatin. At temperatures above 40 °C, gelatin is randomly coiled in aqueous environments, which reversibly forms α-helices and undergoes gelation when the aqueous solution is cooled below 30 °C. Gelatin also retains the RGD motifs present in collagen, which promotes cell adhesion. Furthermore, since gelatin is heat denatured, the concerns of immunogenicity and propagation of pathogens associated with animal-derived collagen are circumvented. For these reasons, gelatin is widely used in tissue engineering applications, and has recently been employed by Berg et al. in 3D bioprinting of human alveolar epithelial models [105,107]. However, the shorter protein lengths and lack of tertiary structure in gelatin, compared to collagen, requires higher protein concentrations (>10 mg/mL) to induce gelation. Since the temperature-dependent, but reversible sol-gel transition of unmodified gelatin poses significant challenges with controlling temperature and viscosity during bioprinting, gelatin is not used in its native state in extrusion 3D bioprinting. These drawbacks can be overcome by either combining gelatin with polymers that undergo ionotropic gelation, as previously described by Berg et al. [105] and De Santis et al. [111], or chemical modification. Native gelatin has been derivatized with unsaturated methacrylamide side groups, which yields the photosensitive derivative, gelatin methacrylamide [117]. Photocrosslinking of gelatin polymers via the methacrylamide carbon double bonds are achieved by UV radiation in the presence of a photoinitiator, such as LAP or Irgacure. Importantly, the physical crosslinks that arise from thermal gelation of gelatin (i.e., at 25 °C) are no longer temperature responsive after covalent UV cross-linking resulting in stiffer gels [118]. Similarly, the derivatization of gelatin with methacrylate groups yields the photosensitive gelatin methacrylate (GelMA), which can also be photo-cross-linked by exposure to UV radiation [119]. Additional control over the extrusion bioprinting of gelatin can be achieved by double functionalization with methacrylation and acetylation, whereby methacrylation controls the mechanical properties of the cross-linked scaffolds, while acetylation controls the rheological properties (viscosity) of the gelatin pregel solution [120].

3.3.5. Silk fibroin

Silk is a fibrous protein derived from the silkworm *Bombyx mori*, and while it has been utilized in the textile industry for centuries, silk fibroin (SF) possesses structural features that make it amenable to the formation of hydrogels. Silk consists of a fibroin core surrounded by sericin proteins, which maintains the structural integrity of the fibrous structure. The fibroin protein is an amphiphilic block copolymer composed of 12 repetitive domains characterized by the sequence G-X-G-X-G-X (G = glycine; X = alanine or serine), and eleven amorphous regions, consisting of more hydrophilic amino acid sequences (Fig. 5E) that separate the predominant hydrophobic clusters. The amphiphilic block copolymer of silk fibroin lends itself to form β-strands [121,122]. Hydrogel formation occurs when the SF transitions from random coils in its sol-state to a gel-state that is composed of crystalline anti-parallel β-sheets. This secondary crystalline structure is stabilized by hydrophobic interactions between the anti-parallel β-sheets and the degree of gelation can be tuned by controlling the protein concentration in solution, temperature, pH, and addition of an organic solvent such a methanol [123,124].

Huang et al. recently 3D bioprinted lung epithelial stem cells (LESCs) using a novel composite hydrogel biomaterial consisting of regenerated silk fibroin (SF) and 2,2,6,6-tetramethylpiperidine-1-oxyl (TEMPO)-oxidized bacterial cellulose (OBC) nanofibrils [125]. The SF backbones were cross-linked using horseradish peroxide/H_2O_2 to form printed hydrogel scaffolds, while OBC was included as a thickener at a concentration of 7% (w/v) to increase the viscosity of the bioink during extrusion and further improve the shape retention of the printed scaffolds. The authors were able to print 3D constructs with ten layers using a composite hydrogel ratio of 1SF:2OBC (SF:OBC = 1:2, w/w). However, the composite hydrogel consisting of 1SF:1OBC (SF:OBC = 1:1, w/w) exhibited a significantly improved compressive strength of 267 ± 13 kPa and a compressive stiffness of 325 ± 14 kPa at 30% strain, respectively. According to SEM and X-ray diffraction analyses, the OBC nanofibrils could also be induced to align along the print lines over 60° of orientation, which provided physical cues for guiding the orientation of LESCs. Importantly, the LESCs maintained their epithelial phenotype and ability to proliferate after 7 days of *in vitro* culture.

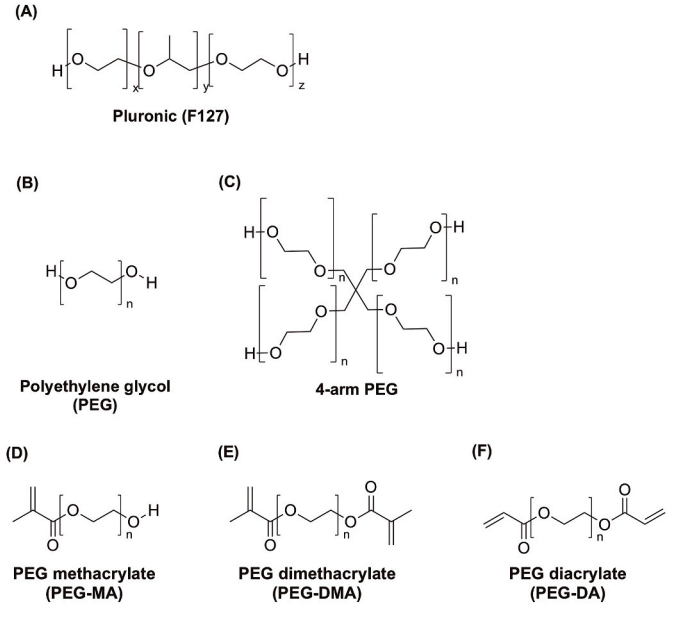

Fig. 6. Chemical structures of synthetic polymers used in the formulation of biomaterial inks and bioinks: (A) Pluronic (F127), (B) polyethylene glycol (PEG), (C) 4-arm PEG, (D) PEG methacrylate (PEG-MA), (E) PEG dimethacrylate (PEG-DMA), and (F) PEG diacrylate (PEG-DA).

3.3.6. Pluronic F127

Pluronic F127 is an important class of biomedical polymers composed of poly(ethylene oxide) (PEO) and poly(propylene oxide) (PPO) arranged as triblock copolymers (PEO-PPO-PEO) (Fig. 6A). The PEO block is hydrophilic and water soluble, whereas the PPO block is hydrophobic and water insoluble. The amphiphilic nature of Pluronic F127 enables it to form micelles by desolvation of the hydrophobic side group of PPO, which interact with each other to form the hydrogel network when the temperature is increased. Its excellent water solubility and thermal responsiveness makes Pluronic F127 an ideal candidate as a sacrificial biomaterial ink when suspended in aqueous solutions. Specifically, Pluronic F127 undergoes a sol-gel transition when the temperature is increased; i.e., a liquid state exists below 10 °C that undergoes gelation at higher temperatures. Falcones et al. [101] exploited Pluronic F127 as a sacrificial bioink to enable 3D bioprinting of tubular structures composed of porcine lung dECM hydrogel that encapsulated mesenchymal stromal cells. Their approach involved printing two concentric rings of Pluronic F127 gel (40% v/v) at room temperature, followed by extrusion of an infill layer composed of porcine lung dECM pregel in between the two Pluronic F127 rings. The process was repeated to construct a tubular structure several layers thick. Thereafter, the 3D constructs were incubated at 37 °C for 30 min to induce gelation of the lung dECM layer. The F127 sacrificial layers were subsequently dissolved by immersing the construct in culture media at 4 °C for 10 min.

3.3.7. Poly(ethylene glycol) or Poly(ethylene oxide)

Poly(ethylene glycol) (PEG) or poly(ethylene oxide) (PEO), is an FDA approved polymer comprising repeating ethylene oxide (C–C–O) units (Fig. 6B and C), and is used in various aspects of biomedical engineering (tissue engineering, nanoparticle-based drug delivery and biosensors) [126]. PEG is innately anti-fouling due to its neutral charge and highly hydrophilic properties. The high water solubility of PEG makes it especially amenable to cell encapsulation and bioprinting applications. However, the PEG polymer alone is incapable of forming physical or chemical networks that are necessary to form hydrogels. Fortunately, the PEG polymer can be functionalized with 'clickable' (i.e., alkynes or azides) and UV-cross-linkable groups (e.g., methacrylate and acrylate) (Fig. 6D–F) to enable the formation of covalent cross-links, in addition to biologically active and cell-adhesive moieties, such as fibronectin-derived RGD peptide, to promote adhesion of encapsulated cells to the PEG polymer network.

Recently, Grigoryan et al. [14] generated novel vascularized lung alveolar models using a 3D bioprintable hydrogel bioink formulation based on PEG-diacrylate (PEGDA) (6 kDa, 20 wt %) via a light-based 3D printing method known as *stereolithography apparatus for tissue engineering* (SLATE). These lung alveolar models were revolutionary in that they consisted of a complex blood vessel network surrounding an artificial air sac that can expand and contract with tidal ventilation. The blood vessel network was perfusable with red blood cells (RBCs) and exhibited bidirectional RBC flow during cyclic ventilation of the enclosed air sac. The authors observed that the hydrogel structure (6 kDa, 20 wt % PEGDA) could withstand more than 10,000 ventilation cycles (24 kPa, 0.5 Hz) over 6 h during RBC perfusion, while switching the inflow gas between humidified oxygen and humidified nitrogen. Unfortunately, this lung alveolar model does not fully recapitulate the microscale architecture of the *in vivo* alveolar air sac, due to the blood vessel network being physically distinct and separate from the air sac which also lacked alveolar epithelial cells, whereas *in vivo*, the alveolar air spaces are in direct contact with their blood capillary networks. Furthermore, the PEG-based hydrogels used to construct this lung alveolar model are likely to elicit potent immune responses of anti-PEG IgM and IgG antibodies and memory T cells, as discussed in the *Biocompatibility* section (3.1.2).

In a separate study to replicate alveolar structures, Lewis et al. took the approach of fabricating photodegradable microsphere templates that were coated with AT2 epithelial cells encapsulated in a thiol-ene

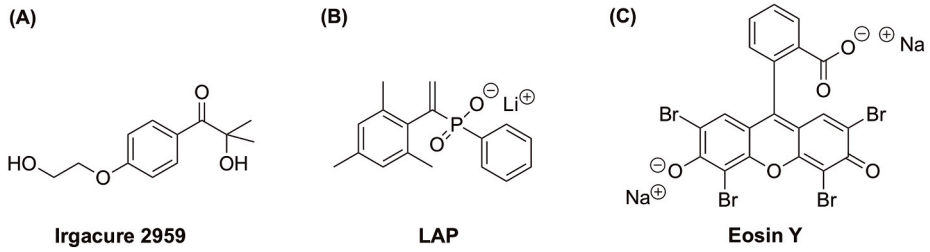

Fig. 7. Chemical structures of commonly used photoinitiators used in covalent crosslinking of acrylate- and methacrylate-functionalized synthetic polymers: (A) Irgacure 2959 ([4-(2-hydroxyethoxy)-phenyl]-2-hydroxy-2-methyl-1-propane-1-one, which absorbs at 257 nm, (B) lithium phenyl(2,4,6-trimethylbenzoyl)phosphinate (LAP), which absorbs at 375 nm and exerts lower cytotoxicity than Irgacure, and (C) Eosin Y (2',4',5',7'-tetrabromo-fluorescein disodium salt), which absorbs at 514 nm (blue visible light) and exerts lower oxidative stress on cells during photoactivation.

hydrogel [127]. The photodegradable microspheres were composed of PEG di-photodegradable acrylate (PEGdiPDA) crosslinked by a photolabile, nitrobenzyl ether crosslinker, which when exposed to 365 nm light, caused cleavage of the crosslinks. Subsequent degradation of the PEGdiPDA microspheres resulted in 120 μm diameter cysts with walls composed of AT2 epithelial cells. These alveolar cysts lacked the hierarchical structure of *in vivo* alveolar sacs as well as an alveolar capillary network. Nonetheless, the individual approaches by Grigoryan et al. [14] and Lewis et al. [127] can conceivably be combined, albeit using different 3D bioprinting techniques to fabricate alveolar sacs comprising AT1 and AT2 epithelial cells with a functionally integrated capillary blood supply.

3.4. Natural and synthetic hydrogel polymers with potential applications to fabricating lung tissue models

3.4.1. Agarose

Agarose is a seaweed-derived linear polysaccharide, which consists of alternating D-galactose and 3,6-anhydro-L-galactopyranose residues, linked by glycosidic bonds (Fig. 5B), with a typical molecular weight of 120 kDa. At temperatures below 45 °C, agarose undergoes thermal liquid-solid phase transition, whereby the inter- and intramolecular hydrogen bonds prevail resulting in the formation of double-stranded helices and trapping of water molecules, which gives rise to a hydrogel [128]. Agarose is used far less frequently than alginate in tissue engineering applications, which is attributed to its low cell attachment property [129]. This shortcoming can be improved upon by combining agarose with collagen [130], whereby the presence of collagen within the agarose polymer network allows the embedded cells to adhere and spread. Another study developed a hybrid bioink comprising agarose (0.5% w/v) and collagen type I (0.2% w/v) for bioprinting of human smooth muscle cells, which exhibited good bioprintability and cytocompatibility [131], and is therefore applicable to the bioprinting of small airways, such as bronchioles, that are lined with smooth muscle fibers.

3.4.2. Gellan gum (Phytagel)

Gellan gum is a water-soluble, anionic polysaccharide (Fig. 5D) produced by the bacterium *Sphingomonas elodea*, which yields a transparent hydrogel. The chemical structure consists of repeating tetrasaccharide units comprising 2 D-Glucose residues, one L-rhamnose residue, and one D-glucuronic acid residue (Fig. 5D) with an average molecular weight of 500 kDa. Like alginate (Fig. 5A), gellan gum also undergoes ionotropic gelation with calcium ions, but at a lower weight percentage of <1% w/v which yields more elastic hydrogels than alginate (undergoes gelation at > 1% w/v). However, in the context of lung tissue fabrication, biomaterial inks composed of gellan gum with greater elasticity will be more conducive to the repeated stretch and relaxation cycles associated with breathing. Similar to alginate, gellan gum also exhibits poor cell adhesion properties. Lozano et al. successfully overcame this drawback by derivatizing gellan gum with RGD, an arginyl-glycyl-aspartyl peptide derived from fibronectin, to create an extrudable biomaterial ink that promoted cell adhesion [132]. Tan et al. used a composite hydrogel ink composed of gellan gum and polyvinylalcohol (PVA), and developed a cryogenic printing technique to print complex 3D geometrical structures with mechanical properties that mimic the softest tissues found in the human body, such as the brain and lungs [133]. Furthermore, this material was found to be compatible with collagen type I, an ECM protein component, which has been used by Berg et al. in combination with alginate and gelatin to fabricate alveolar epithelial tissue models [107].

3.4.3. Fibrin

Fibrin is a fibrous protein and component of natural ECM, which is formed by the catalytic polymerization of fibrinogen (~340 kDa) by thrombin, a key reaction that initiates blood coagulation [134]. Fibrinogen is a glycoprotein that consists of multiple pairs of polypeptide chains: Aα, Bβ, and γ. Thrombin-catalyzed cleavage of the Aα and Bβ chains forms fibrino-peptide A and B monomers, which then spontaneously polymerize into protofibrils and self-associate laterally into fibrin fibers. The fibrin fibers subsequently associate to form fibrin gel [135]. The rapid, predictable and straightforward gelation process makes the pairing of fibrinogen and thrombin a convenient two-component biomaterial ink. In addition, fibrin has innate cell adhesion motifs and is biodegradable, which are key factors that make it particularly useful as a sacrificial biomaterial ink that can potentially be used to fabricate hollow tubes as bronchioles and microsphere cysts as alveoli and alveolar sacs. While fibrin-based 3D scaffolds were found to promote cell adhesion and proliferation, the fibrin hydrogels were fragile and soft, and had difficulty maintaining its structure [136]. It should be emphasized that, in comparison with alginate-only scaffolds, fibrin has an advantage in terms of biocompatibility. The drawback of fibrin-based hydrogels can be overcome by combining the fibrinogen pregel with other physical or chemical cross-linkable polymers as outlined in Table 3.

3.4.4. Micro- and nanogels

As discussed earlier in section 3.1.5, hydrogels are water swollen polymer networks that can be synthesized in several different ways and applied to various important areas [137]. Microgels/nanogels [138–141] are hydrogel particles that have diameters ranging from tens of nanometers to several micrometers depending on the synthetic conditions. Nanogels are typically thought of as having diameters <100 nm, while the diameter of microgels are >100 nm. The first microgel particles were prepared by Staudinger and Husemann [142] over 70 years ago. The term 'microgel' was introduced by Baker [143] in 1949 and poly(DVB) was the first microgel prepared in an organic solvent at high dilution. Microgel research expanded considerably after the discovery of thermal responsive poly(N-isopropylacrylamide) (pNIPAm) microgels by Pelton and Chibante in 1986 [144]. Microgels/nanogels that are responsive to temperature [145], pH [146], magnetic fields [147], electric fields [148], metals [149], small molecules [150] and ionic strength [151] have emerged as important moieties for sensing [152], chemical separation [153], and drug delivery [154–156]. Additionally, individual microgels/nanogels can be made responsive to multiple stimuli by incorporating functional monomers into the pNIPAm

backbone during the synthesis to yield microgels/nanogels with the desired combined functionality. For example, pNIPAm microgels can be rendered responsive to pH or glucose by adding functional monomers such as acrylic acid (AAc) [157], 2-hydroxyethyl methacrylate [158], N-[3-(dimethylamino)propyl]-methacrylamide [159] or 3-(acrylamido) phenylboronic acid [156]. Microgels offer some advantages compared to normal particulate drug carrier dispersions, such as, superior colloidal stability, ease of preparation, size controllability and convenience of functionalization.

The abovementioned advantages of microgels can be leveraged to overcome the challenges associated with developing biomaterial inks for extrusion-based bioprinting. As discussed earlier, 3D bioprintable materials have to be both nontoxic and compatible with printing processes [160,161]. In particular, a biomaterial ink must flow from a reservoir onto a print surface and then rapidly stabilize to preserve fidelity of the printed structure relative to the computer design in extrusion printing [162,163]. Non-viscous precursor solutions, such as PEG [164] and hyaluronic acid (HA) [165] are attractive materials for bioinks due to their ability to encapsulate cells and biomolecular materials for tissue engineering applications. However, their poor stability and shape fidelity poses a significant challenge. Among these printable materials, hydrogels have long been valuable in the engineering of tissues, due to their tunable biophysical and biochemical properties and their ability to encapsulate cells with a high water content [166]. However, hydrogels can be challenging to print without additional modification or the use of additives that serve as thickeners [167].

In order to overcome these limitations, microgels have been adapted for 3D printing applications to create more defined and complex scaffolds. To enable printing through extrusion-based printing methods, microgel bioinks are loaded into syringes, subjected to large pressures and/or high temperatures, and extruded out of a nozzle onto a surface. However, this technique also has limitations due to the high levels of shear stress and high temperatures associated with the extrusion process damaging cells and other biological components incorporated within the bioink [161,168]. Furthermore, extrusion-based printing techniques commonly use microgel particles with diameters from 30 to 200 μm to avoid small needle gauges that would further increase the shear stress that occurs during extrusion-based printing. Therefore, other printing techniques [169] that are less damaging to cells, as well as encapsulated biological components, which can also be used to print significantly smaller particles need to be explored (Table 2).

Techniques used in other industries that have the potential to be adapted for the purpose of creating microgel-based scaffolds can solve the limitations presented by conventional bioprinting techniques. For example, ultrasonic microplotting, has primarily been used for the printing of patterned individual molecular arrangements, such as DNA, proteins, or small molecules in a solvent [170]. This technique uses a piezoelectric element attached to a glass capillary write head to print inks onto a surface in a non-contact manner. When the piezoelectric element is operational, an ultrasonic wave changes the surface tension and wetting behavior between the resident ink and dispensing tip, causing a bead of ink to form at the dispensing tip, which is brought into contact with the substrate and preferentially wets and prints on the desired substrate. The advantages of this printing process is that it does not require the high heat, temperatures, or pressures that are commonly associated with other scaffold fabrication techniques, such as electrospinning, certain lithography methods, and extrusion-based printing, which have the potential to damage the cellular constituents and often restricts the inclusion of biological molecules. Chester et al. [171] developed an ultrasonic microplotting technique to create patterned microgel films. By optimizing the printing parameters, such as bioink formulation, surface contact angle, and print head diameter, the authors successfully prepared printed microgel films. Microgel particles were synthesized in a precipitation-polymerization reaction and mixed with low molecular weight PEG (i.e., PEG 400) to produce the microgel-based bioinks used for ultrasonic microplotting. Using a cyanoacrylate adhesive, the piezoelectric element was attached to a glass capillary to print microgel bioinks using ultrasonic microplotting. Ultrasonic waves generated from piezoelectric element change the surface tension and wetting behavior to establish the connection between the microgel solution and substrate.

An alternate approach to developing biomaterial inks involves the use of jammed microgels, which were initially introduced by Highley et al. for 3D printing applications [172]. Jammed microgels can be designed into both surface features and 3D structures within hydrogel supports, and further stabilized with secondary cross-linking such as, thiol-ene cross-linked hyaluronic acid (HA), photo-cross-linked PEG, and thermosensitive agarose. Furthermore, cells can be easily incorporated into the jammed microgels without decreasing their viability. The versatility of this particle-based approach opens up numerous potential biomedical applications through the printing of a more diverse set of inks.

An attractive advantage of jammed microgel bioinks is their ability to overcome the exposure of cells to excessive shear stresses during printing to form a colloidal-like suspension. Sometimes, the microgel matrix environment can support and optimize the 3D printed structures. In one study, Zhang et al. [173] described a method for 3D printing large-scale extracellular matrix (ECM) structures made from collagen type I at the relatively low concentrations often used in 3D cultures. Jammed granular-scale microgels were used as a 3D printing support medium. Compared to previously used hydrogel structures, granular-scale microgels are more tightly packed. Printing collagen type I directly into microgels results in structures with well-defined features within a range of operating parameters.

PEG-based microgels have also been developed using various methods. For example, Xin et al. reported a novel bioink consisting of PEG microgels prepared via off-stoichiometry thiol–ene click chemistry [174]. Interparticle adhesion forces enable the microgel bioink to be easily extruded and exhibit excellent stability after printing. Furthermore, the microgel bioinks can be photochemically annealed with a second cross-linking reaction to confer long-term stability to printed constructs. PEG microgel-based bioinks have highly tunable physicochemical properties and advanced modularity. The low forces required for extrusion and cytocompatibility of the thiol-ene chemistry enables the incorporation of cells with high viability. The cells were able to spread and proliferate in the spaces between microgels even after the structures were annealed. Overall, these results indicate that microgel bioinks are a promising and versatile platform that could be leveraged for bioprinting and regenerative manufacturing.

Other polymeric materials, like oxidized methacrylated alginate (OMA) hydrogels, have demonstrated the ability to support cell infiltration and migration. Jeon et al. generated alginate-based microgels for cell encapsulation and tissue construction [175]. Microgels were prepared with calcium ion cross-linked methacrylated-alginate, and then further photo-cross-linked using UV light. Based on this principle, they scaled up and structured large and complex biological tissues with predefined geometrical features that are capable of encapsulating cells; i.e., human bone marrow-derived mesenchymal stem cells (hMSCs). Microgel encapsulated hMSCs also maintained high cell viability after 4 weeks in spinner flask culture. Furthermore, these cell-laden microgels could be directly assembled while maintaining high cell viability.

Microgels/nanogels have also been used as building blocks for biofabrication. They are assembled into 3D constructs using an automated assembly technology, or bioprinting to develop both *in vitro* models and implantable constructs that mimic the complexity of native tissues. Traditionally, extrudable bioinks are prepared using single or double network hydrogels, and their biophysical and biochemical properties are kept homogeneous, although, heterogeneity may be desirable for printing complex tissues. To address this limitation, microgels/nanogels can be combined with an extrudable bulk hydrogel precursor to engineer a composite bioink platform containing distinct microscale and macroscale environments.

More advanced technologies should be focused on the development of a diverse set of multifunctional bioinks in which the local microenvironment can be tailored for distinct encapsulated cell types or bioactive factors. Biomaterial inks for extrusion bioprinting have generally been engineered at the molecular scale, often leveraging reversible cross-linking chemistries. However, the shear thinning behavior of microgels/nanogels is based predominately on the physical interactions between particles, which expand the range of materials that can be extruded. Another advantage of microgel/nanogel-based biomaterial inks is their inherent modularity in which multiple particle populations can be fabricated and then 'jammed' together.

In general, traditional extrusion bioprinting approaches involve layer-by-layer printing onto a 2D surface, thus making it challenging to print complex 3D structures. To overcome this limitation, gel printing approaches have been developed in which biomaterial inks are directly extruded into a secondary support hydrogel that serves to minimize the effect of gravity. This enables the printing of taller, more complex 3D structures. Microgel/nanogel systems are an ideal support for gel-in-gel printing, because the particles around the translating nozzle locally displace to support the biomaterial ink and printed object. A commonly used support hydrogel for 3D printing is Carbopol, which is a commercial, particle-based hydrogel composed of poly(acrylic acid) microgels (average diameter 0.2 μm). Carbopol-support hydrogels are compatible with a wide range of bioinks and can be used to print diverse, multicellular structures. Support hydrogels for 3D printing have also been made using a granular gelatin microgel system prepared by fragmentation.

The use of microgels/nanogels for 3D bioprinting is still in its infancy, with jammed microgels systems predominantly leveraged for extrusion bioprinting. The shear-thinning behavior of jammed microgels is based on the physical interactions between the particles. Thus, the range of materials that can be processed by extrusion printing will likely expand. In addition, the modularity of microgels/nanogels systems may enable the preparation of more diverse inks with multifunctional behaviors. Microgels composed of different chemistries can be controllably mixed together, in various ratios, to tune the composition of the inks. Another great benefit of microgels is their ability to load and release small molecules in a triggered fashion. These molecules can be bioactive themselves, and the microgels can be programmed to release these molecules in response to a myriad of stimuli, e.g., presence of enzymes that break polymer bonds to release small molecules. Further advances in this area will enable high-resolution positioning within 3D systems, which will be highly beneficial to replicating the intricate lung airway architecture, particularly at the level of bronchioles, alveolar sacs and individual alveoli.

3.4.5. *Self-assembling biomaterial inks*

Supramolecular materials encompass architectures consisting of molecules that are able to self-assemble into larger constructs via non-covalent interactions [176]. The self-assembled structures can be formed from polymers that have functional groups that can participate in non-covalent bonding interactions directly incorporated into the polymer backbone, at the termini, or as pendant groups that can form non-covalent crosslinks. Supramolecular materials can also be formed from small molecules, i.e., low molecular weight gelators (LMWGs), which are programmed with chemical information to undergo self-assembly and/or molecular recognition interactions into polymeric structures. Although many bioinks with supramolecular polymeric materials have been developed [177], little work has been done with small molecule gelators. Gelators for water include cross-linked inorganic and organic polymers as well as small molecules, often referred to as LMWGs. LMWGs gel water mostly via the self-assembly of 1D aggregates (i.e., fibers) that can arrange into a volume spanning network, driven exclusively by the formation of noncovalent interactions (i.e., physical cross-links). LMWGs may also form gels via networks of sheet-like structures, although those cases are rare [178].

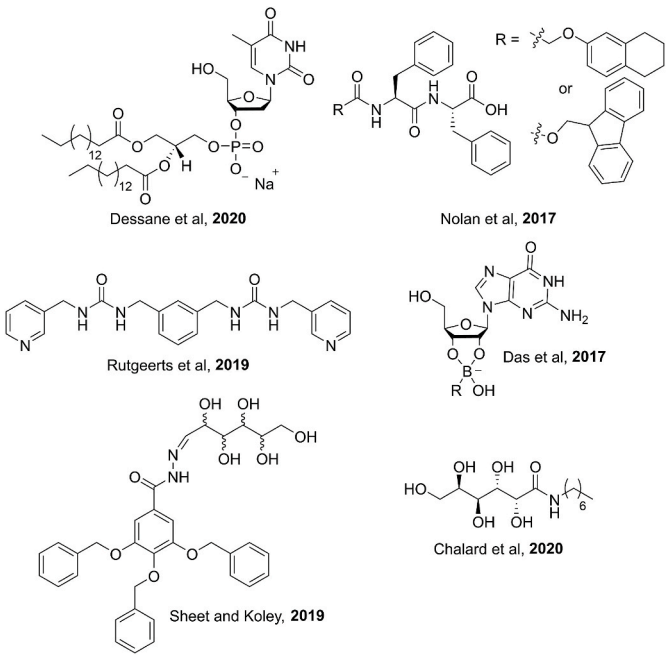

Fig. 8. Chemical structures of 3D printable low molecular weight gelators.

While natural polymers suffer drawbacks such as compositional variation (i.e., collagen), other polymer systems include poor biocompatibility, high hydrophilicity, high hydrophobicity, high melting points, slow cross-linking, as well as the presence of undesired air bubbles and inhomogeneities in the resulting 3D printed structures. Existing formulations of natural and synthetic polymers are also useful for only specific applications and thus progress in the field is hampered by lack of bigger variety of printable hydrogel systems [29,179,180]. In contrast, LWMGs offer numerous attractive features such as synthetic tunability, ease of preparation, lower gelator concentrations (i.e., "supergelators" <0.1 wt %), biodegradability, biocompatibility, reversible gelation, and responsiveness to a variety of stimuli, including heat, light, sound, mechanical shear, chemicals, and pH [181]. Also, the rheological properties of gels from LMWGs can be tunable by adjusting the self-assembly conditions [182] in order to potentially meet the demands of bioinks for specific applications, such as printing lung tissue models.

Although supramolecular gels from LWMGs are not as mechanically robust as natural or synthetic polymer gels, the thixotropic and self-healing potential of LMWGs can be advantageous for dispersed cells, as well as during the printing process [29]. Many gels from LMWGs exhibit sheer thinning behavior upon application of a mechanical sheer such as the sheering force applied through a syringe. Upon applying mechanical sheer with a syringe, the gel exhibits sheer thinning property and eventually flows to enable printing, after which the self-healing properties come into play as the printed gel reforms in order to hold its shape on the substrate. The following examples in this section summarize a few recent developments towards incorporating LMWGs into bioink and biomaterials ink formulations. Although these examples do not directly involve 3D printing lung tissue constructs, they are included as a starting point to inspire the development of these fascinating materials towards applications in future 3D printable bioinks and biomaterial inks for lung tissue constructs.

Although the potential of LWMGs for cell scaffolds, molding and printing 3D shapes has been recognized [183], the first biomaterial ink from a LMWG has only been very recently reported by Dessane et al. [180]. A nucleotide lipid-based LMWG (Fig. 8) was used to form hydrogels with fast gelation kinetics in a cell culture medium with shear moduli and thixotropy, compatible with extruded oral cell survival

Table 4
Comparison of natural and synthetic polymer hydrogels with potential applications to fabricating lung tissue models.

Biomaterial	Polymer Type	Gelation Mechanism	Compatible Bioprinting Method	Potential Function[a]	Potential Lung Tissue Applications
Agarose [128–131]	Natural, Polysaccharide	Thermo-responsive (Gelation at < 45 °C)	Extrusion-based deposition	Sacrificial	Bronchioles, Alveolar sacs, Alveoli
Gellan Gum [132,133]	Natural, Polysaccharide	Ionic crosslinking	Extrusion- and Inkjet-based deposition	Structural, Sacrificial	Alveolar sacs, Alveoli
Fibrin [134–136]	Natural, Protein	Polymerization (enzymatically catalyzed by thrombin)	Extrusion-based deposition	Functional, Sacrificial	Bronchioles, Alveolar sacs, Alveoli
Micro- and Nanogels [137–150] [151–175]	Natural (Oxidised methacrylated alginate, Collagen type I), Synthetic (PEG)	Ionic crosslinking, Click-reactions, Chemical crosslinking, Dynamic crosslinking	Injection Self-assembly	Structural, Tissue adhesion, Self-healing, Sacrificial	Bronchioles, Alveolar sacs, Alveoli
Self-Assembling Biomaterial Inks [176–187]	Synthetic	Self-assembly	Extrusion-based deposition	Sacrificial	Bronchioles, Alveolar sacs, Alveoli

[a] Refer to footnotes of Table 3 for definitions of biomaterial ink functions.

(human gingival fibroblasts and stem cells from apical papilla). The nucleotide lipid-based gelator was synthesized in one step from commercially available reagents with an acceptable yield (47%) [180].

Nolan et al. reported 3D printable hydrogels from diphenylalanine dipeptide (diPhe) derivatives, where gelation was triggered by solvent as well as pH [184] (Fig. 8). Although no studies were carried out with cells, the diPhe derivative hydrogels could be promising components in future bioinks. In another study, Rutgeerts et al. reported a bis-urea derivative which is compatible with L929 fibroblasts, but no printing was done with this material [185] (Fig. 8). Self-healable hydrogels based on arylboronate esters of G-quadruplexes were reported by Das et al. which were biocompatible with adult human dermal fibroblast cells and was demonstrated as a promising candidate for biomaterial inks [179] (Fig. 8). In other related work, Sheet and Koley successfully fabricated a 3D printed bacterial microhabitat using a hydrogel from a glucose-modified dendron compound [186] (Fig. 8). Chalard et al. developed a method to 3D print supramolecular hydrogels from an *N*-heptyl-D-galactonamide derivative, however, no work with cells was done [187] (Fig. 8). 3D printed structures were generated from an organogel of the N-heptyl-D-galactonamide with DMSO, which were set via solvent exchange with water [187]. The method is amenable to non-thixotropic gels and cells could be incorporated into the resulting hydrogel constructs. Given the diversity in the chemical structures of the LWMGs in the examples described in this section, which is a small fraction of all LMWGs that have been reported to date, there exists vast potential to design and synthesize other LMWGs with fascinating and desirable properties. Undoubtedly, these materials may play a key role in future bioinks and biomaterial inks for 3D printed lung tissue constructs (Table 4).

4. Challenges and future directions

Lung tissue bioprinting is still in early development and, as such, there is still a lot of potential for improvement. In this review we have explored how the complexity of lung architecture and structure makes it an extremely difficult organ to replicate using conventional bioprinting approaches. This is largely due to the fact that most of the currently available bioinks do not meet all the requirements for the fabrication of the complex lung tissue scaffold, i.e., strength, elasticity, promotion of cell adhesion and biodegradability and it is mainly due to this lack of a biocompatible, yet versatile bioink that 3D bioprinting of lung tissue has been relatively slower compared to some other organs.

In our view, 3D bioprinting of lung tissues is going to advance in three main areas over the next couple of decades: (1) development of multifunctional biomaterial inks, (2) design of immunocompetent lung tissues and structures, and (3) 3D bioprinting lung tissues that can be transplanted into patients with lung disease.

(1) Although various 3D bioprinting technologies have been successfully applied over the last few decades, they have largely relied on natural polymers such as alginate, gelatin and hyaluronic acid. It is only in the last decade that large strides in biomaterial ink design have only occurred with the development of synthetic inks and bioinks that have multiple properties and biocompatibility with lung tissue cells. The development of new and multifunctional bioinks such as synthetic and composite polymer hydrogels, and advanced materials, such as micro- and nano-structured biomaterial inks will be necessary to further advance the field of lung 3D bioprinting. In particular, we envision that the next horizon will be the design of “smart” materials that not only form the matrix of the 3D bioprinted lung tissue but can sense and respond to biological signals. For example, a matrix material that can change viscoelastic properties based on the release of cell enzymes and inflammatory mediators would allow for the formation of a more robust lung tissue.
(2) Much of lung disease research explores pathological conditions that rely on an immunocompetent system in which the major immune cells such as neutrophils, mast cells, macrophages and lymphocytes are able to modify lung physiology. A matrix material that is able to sustain immune cell migration and differentiation is essential to produce an immunocompetent lung organ that can respond to inflammatory signals. The design of an immunocompetent 3D lung tissue model would propel drug development ahead significantly. Similarly, bioinks that are able to sense danger signals such as pathogens and then release mediators to regulate localized immune responses would mimic physiological responses and make the bioprinted lung much more appropriate for use in this type of research.
(3) Current lung transplant procedures replace unhealthy lung tissue with a healthy tissue from a donor. The lung recipient patient is then placed on immunosuppressant medication to prevent organ rejection. It is, therefore, attractive to produce 3D bioprinted lung tissue using the recipients own stem cells, thereby bypassing the potential for rejection. Recent advances in pluripotent stem cell technology have allowed for the differentiation of many cell types, including most of the cell types that comprise the lung tissue. It is still a very distant objective to produce an entire lung organ. However, it may be possible to 3D bioprint an alveolus or a section of the bronchi, and thereby allow for transplantation. Surgical advances will need to accompany any such advances in 3D bioprinting.

5. Conclusion

Recent advances in biofabrication, tissue engineering, regenerative medicine and additive manufacturing have demonstrated the potential to create *in vitro* tissue models that recapitulate the intricate ultrastructure of *in vivo* lung tissue. At the confluence of the abovementioned disciplines, extrusion-based bioprinting and stereolithography have demonstrated considerable potential in the endeavor to biofabricate viable *in vitro* lung tissue models. However, these 3D bioprinting modalities, as well as their associated biomaterial inks and bioinks, still have scope for improvement with respect to enhancing the spatial control of cellular and ECM deposition and resolution of the 3D printed tissue structures. This is especially crucial in the context of lung tissue since its ability to facilitate air conduction and gaseous exchange with the circulatory system is inextricably linked with its intricate anatomical and tissue ultrastructure. The future of lung 3D bioprinting may indeed entail hybrid approaches that exploit several different bioprinting modalities and biomaterial inks/bioinks to biofabricate and assemble various parts of the lung airway system from the trachea to individual alveoli with integrated blood vasculature into a contiguous, functional network. Furthermore, reliable cell sources for each type of lung epithelial layer, including ciliated epithelium of the trachea and bronchi to the alveolar epithelium, must also be established. This need may be met by allogeneic donor populations or host-derived pluripotent stem cells. Additionally, the 3D bioprinted structures need to maintain lumen patency throughout all levels of the pulmonary airway system, as well as its associated vasculature. Hence, the evolution of biomaterial ink/bioink chemistries and compositions that combine the features of sacrificial biomaterials, such as LMWGs, and advantages of microgels/nanogels will certainly play a key role in advancing the 3D bioprinting of biomimetic lung tissue models.

Funding

This work was funded by the National Research Council Canada.

CRediT authorship contribution statement

Leshern Karamchand: Conceptualization, Writing – original draft, Writing – review & editing. **Darren Makeiff:** Conceptualization, Writing – original draft, Writing – review & editing. **Yongfeng Gao:** Writing – original draft, Writing – review & editing. **Khalid Azyat:** Writing – original draft, Writing – review & editing. **Michael J. Serpe:** Writing – review & editing. **Marianna Kulka:** Conceptualization, Funding acquisition, Supervision, Writing – original draft, Writing – review & editing.

Declaration of competing interest

The authors declare that they have no known competing financial interests or personal relationships that could have appeared to influence the work reported in this paper.

Data availability

This review is an appraisal of published data from the literature relevant to the biofabrication of lung tissue models.

Acknowledgements

The authors thank Ashley Wagner for her insightful feedback and maintaining an upbeat atmosphere in the lab with the music of ABBA and Cher during the writing of this manuscript.

References

[1] M. Guvendiren, 3D Bioprinting in Medicine, Springer International Publishing, Cham, 2019, https://doi.org/10.1007/978-3-030-23906-0.
[2] A. O'Dowd, Peers call for UK to harness "enormous" potential of regenerative medicine, BMJ 347 (2013) f4248, https://doi.org/10.1136/bmj.f4248.
[3] J. Groll, T. Boland, T. Blunk, J.A. Burdick, D.W. Cho, P.D. Dalton, B. Derby, G. Forgacs, Q. Li, V.A. Mironov, L. Moroni, M. Nakamura, W. Shu, S. Takeuchi, G. Vozzi, T.B.F. Woodfield, T. Xu, J.J. Yoo, J. Malda, Biofabrication, Reappraising the definition of an evolving field, Biofabrication 8 (2016), https://doi.org/10.1088/1758-5090/8/1/013001.
[4] S.V. Murphy, A. Atala, 3D bioprinting of tissues and organs, Nat. Biotechnol. 32 (2014) 773–785, https://doi.org/10.1038/nbt.2958.
[5] J. Groll, J.A. Burdick, D.W. Cho, B. Derby, M. Gelinsky, S.C. Heilshorn, T. Jüngst, J. Malda, V.A. Mironov, K. Nakayama, A. Ovsianikov, W. Sun, S. Takeuchi, J. J. Yoo, T.B.F. Woodfield, A definition of bioinks and their distinction from biomaterial inks, Biofabrication 11 (2019), https://doi.org/10.1088/1758-5090/aaec52.
[6] H. Cui, M. Nowicki, J.P. Fisher, L.G. Zhang, 3D bioprinting for organ regeneration, Adv. Healthc. Mater. 6 (2017), https://doi.org/10.1002/adhm.201601118.
[7] J.-S. Lee, H. Do Cha, J.-H. Shim, J.W. Jung, J.Y. Kim, D.-W. Cho, Effect of pore architecture and stacking direction on mechanical properties of solid freeform fabrication-based scaffold for bone tissue engineering, J. Biomed. Mater. Res. A. 100 (2012) 1846–1853, https://doi.org/10.1002/jbm.a.34149.
[8] M.I. Gariboldi, S.M. Best, Effect of ceramic scaffold architectural parameters on biological response, Front. Bioeng. Biotechnol. 3 (2015) 151, https://doi.org/10.3389/fbioe.2015.00151.
[9] G. Ahn, J.H. Park, T. Kang, J.W. Lee, H.-W. Kang, D.-W. Cho, Effect of pore architecture on oxygen diffusion in 3D scaffolds for tissue engineering, J. Biomech. Eng. 132 (2010), 104506, https://doi.org/10.1115/1.4002429.
[10] H. Kang, C.-Y. Lin, S.J. Hollister, Topology optimization of three dimensional tissue engineering scaffold architectures for prescribed bulk modulus and diffusivity, Struct. Multidiscip. Optim. J. Int. Soc. Struct. Multidiscip. Optim. 42 (2010) 633–644, https://doi.org/10.1007/s00158-010-0508-8.
[11] D. Huh, B.D. Matthews, A. Mammoto, M. Montoya-Zavala, H.Y. Hsin, D.E. Ingber, Reconstituting organ-level lung functions on a chip, Science 328 (2010) 1662–1668, https://doi.org/10.1126/science.1188302.
[12] H.C. Ott, B. Clippinger, C. Conrad, C. Schuetz, I. Pomerantseva, L. Ikonomou, D. Kotton, J.P. Vacanti, Regeneration and orthotopic transplantation of a bioartificial lung, Nat. Med. 16 (2010) 927–933, https://doi.org/10.1038/nm.2193.
[13] T.H. Petersen, E.A. Calle, L. Zhao, E.J. Lee, L. Gui, M.B. Raredon, K. Gavrilov, T. Yi, Z.W. Zhuang, C. Breuer, E. Herzog, L.E. Niklason, Tissue-engineered lungs for in vivo implantation, Science 329 (2010) 538–541, https://doi.org/10.1126/science.1189345.
[14] B. Grigoryan, S.J. Paulsen, D.C. Corbett, D.W. Sazer, C.L. Fortin, A.J. Zaita, P. T. Greenfield, N.J. Calafat, J.P. Gounley, A.H. Ta, F. Johansson, A. Randles, J. E. Rosenkrantz, J.D. Louis-Rosenberg, P.A. Galie, K.R. Stevens, J.S. Miller, Multivascular networks and functional intravascular topologies within biocompatible hydrogels, 80-, Science 364 (2019) 458–464, https://doi.org/10.1126/science.aav9750.
[15] S.P. Tarassoli, Z.M. Jessop, S. Kyle, I.S. Whitaker, Candidate Bioinks for 3D Bioprinting Soft Tissue, Elsevier Ltd., 2018, https://doi.org/10.1016/B978-0-08-101103-4.00026-0.
[16] M.G. Levitzky, Pulmonary Physiology, 9e, in: Pulm. Physiol. 9e, 9e ed., The McGraw-Hill Companies, Inc., 2017.
[17] E.R. Weibel, D.M. Gomez, Architecture of the human lung, 80-, Science 137 (1962) 577–585, https://doi.org/10.1126/science.137.3530.577.
[18] R.R. Mercer, M.L. Russell, J.D. Crapo, Alveolar septal structure in different species, J. Appl. Physiol. 77 (1994) 1060–1066, https://doi.org/10.1152/jappl.1994.77.3.1060.
[19] A. Makanya, A. Anagnostopoulou, V. Djonov, Development and remodeling of the vertebrate blood-gas barrier, 2013, BioMed Res. Int. (2013) 1–15, https://doi.org/10.1155/2013/101597.
[20] M. Ochs, J.R. Nyengaard, A. Jung, L. Knudsen, M. Voigt, T. Wahlers, J. Richter, H. J.G. Gundersen, The number of alveoli in the human lung, Am. J. Respir. Crit. Care Med. 169 (2004) 120–124, https://doi.org/10.1164/rccm.200308-1107OC.
[21] M.M.-J. Chang, L. Shih, R. Wu, Pulmonary epithelium: cell types and functions, in: Pulm. Ep. Heal. Dis., John Wiley & Sons, Ltd, Chichester, UK, 2008, pp. 1–26, https://doi.org/10.1002/9780470727010.ch1.
[22] V.V. Thacker, N. Dhar, K. Sharma, R. Barrile, K. Karalis, J.D. McKinney, A lung-on-chip model of early m. Tuberculosis infection reveals an essential role for alveolar epithelial cells in controlling bacterial growth, Elife 9 (2020) 1–73, https://doi.org/10.7554/eLife.59961.
[23] J.C. Bonner, Molecular mechanisms of respiratory toxicity, in: R.C. Smart, E. Hodgson (Eds.), Mol. Biochem. Toxicol, fifth ed., John Wiley & Sons, New York, 2018, pp. 591–628, fifth ed.
[24] J.E. Nichols, J.A. Niles, S.P. Vega, L.B. Argueta, A. Eastaway, J. Cortiella, Modeling the lung: design and development of tissue engineered macro- and micro-physiologic lung models for research use, Exp. Biol. Med. 239 (2014) 1135–1169, https://doi.org/10.1177/1535370214536679.
[25] P. Bajaj, J.F. Harris, J.-H. Huang, P. Nath, R. Iyer, Advances and challenges in recapitulating human pulmonary systems: at the cusp of biology and materials, ACS Biomater. Sci. Eng. 2 (2016) 473–488, https://doi.org/10.1021/acsbiomaterials.5b00480.

[26] M.L. Bedell, A.M. Navara, Y. Du, S. Zhang, A.G. Mikos, Polymeric systems for bioprinting, Chem. Rev. 120 (2020) 10744–10792, https://doi.org/10.1021/acs.chemrev.9b00834.

[27] L. Valot, J. Martinez, A. Mehdi, G. Subra, Chemical insights into bioinks for 3D printing, Chem. Soc. Rev. 48 (2019) 4049–4086, https://doi.org/10.1039/c7cs00718c.

[28] M. Mobaraki, M. Ghaffari, A. Yazdanpanah, Y. Luo, D.K. Mills, Bioinks and bioprinting: a focused review, Bioprinting 18 (2020), e00080, https://doi.org/10.1016/j.bprint.2020.e00080.

[29] T. Jungst, W. Smolan, K. Schacht, T. Scheibel, J. Groll, Strategies and molecular design criteria for 3D printable hydrogels, Chem. Rev. 116 (2016) 1496–1539, https://doi.org/10.1021/acs.chemrev.5b00303.

[30] S.W. Bae, K.W. Lee, J.H. Park, J.H. Lee, C.R. Jung, J.J. Yu, H.Y. Kim, D.H. Kim, 3D bioprinted artificial trachea with epithelial cells and chondrogenic-differentiated bone marrow-derived mesenchymal stem cells, Int. J. Mol. Sci. 19 (2018) 1–14, https://doi.org/10.3390/ijms19061624.

[31] J.H. Park, J.K. Yoon, J.B. Lee, Y.M. Shin, K.W. Lee, S.W. Bae, J.H. Lee, J.J. Yu, C. R. Jung, Y.N. Youn, H.Y. Kim, D.H. Kim, Experimental tracheal replacement using 3-dimensional bioprinted artificial trachea with autologous epithelial cells and chondrocytes, Sci. Rep. 9 (2019) 1–11, https://doi.org/10.1038/s41598-019-38565-z.

[32] R. Kaye, T. Goldstein, D.A. Grande, D. Zeltsman, L.P. Smith, A 3-dimensional bioprinted tracheal segment implant pilot study: rabbit tracheal resection with graft implantation, Int. J. Pediatr. Otorhinolaryngol. 117 (2019) 175–178, https://doi.org/10.1016/j.ijporl.2018.11.010.

[33] A. Copploe, M. Vatani, J.W. Choi, H. Tavana, A three-dimensional model of human lung airway tree to study therapeutics delivery in the lungs, Ann. Biomed. Eng. 47 (2019) 1435–1445, https://doi.org/10.1007/s10439-019-02242-z.

[34] B.C. Gross, J.L. Erkal, S.Y. Lockwood, C. Chen, D.M. Spence, Evaluation of 3D printing and its potential impact on biotechnology and the chemical sciences, Anal. Chem. 86 (2014) 3240–3253, https://doi.org/10.1021/ac403397r.

[35] M.W. Tibbitt, K.S. Anseth, Hydrogels as extracellular matrix mimics for 3D cell culture, Biotechnol. Bioeng. 103 (2009) 655–663, https://doi.org/10.1002/bit.22361.

[36] H. Geckil, F. Xu, X. Zhang, S. Moon, U. Demirci, Engineering hydrogels as extracellular matrix mimics, Nanomedicine 5 (2010) 469–484, https://doi.org/10.2217/nnm.10.12.

[37] M. Guvendiren, J. Molde, R.M.D. Soares, J. Kohn, Designing biomaterials for 3D printing, ACS Biomater. Sci. Eng. 2 (2016) 1679–1693, https://doi.org/10.1021/acsbiomaterials.6b00121.

[38] A.J. Booth, R. Hadley, A.M. Cornett, A.A. Dreffs, S.A. Matthes, J.L. Tsui, K. Weiss, J.C. Horowitz, V.F. Fiore, T.H. Barker, B.B. Moore, F.J. Martinez, L.E. Niklason, E. S. White, Acellular normal and fibrotic human lung matrices as a culture system for in vitro investigation, Am. J. Respir. Crit. Care Med. 186 (2012) 866–876, https://doi.org/10.1164/rccm.201204-0754OC.

[39] E.S. White, Lung extracellular matrix and fibroblast function, Ann. Am. Thorac. Soc. 12 (2015), https://doi.org/10.1513/AnnalsATS.201406-240MG. S30–S33.

[40] G. Burgstaller, B. Oehrle, M. Gerckens, E.S. White, H.B. Schiller, O. Eickelberg, The instructive extracellular matrix of the lung: basic composition and alterations in chronic lung disease, Eur. Respir. J. 50 (2017), https://doi.org/10.1183/13993003.01805-2016.

[41] B. Suki, J.H.T. Bates, Extracellular matrix mechanics in lung parenchymal diseases, Respir. Physiol. Neurobiol. 163 (2008) 33–43, https://doi.org/10.1016/j.resp.2008.03.015.

[42] D.S. Faffe, W.A. Zin, Lung parenchymal mechanics in health and disease, Physiol. Rev. 89 (2009) 759–775, https://doi.org/10.1152/physrev.00019.2007.

[43] J.E. Wagenseil, R.P. Mecham, New insights into elastic fiber assembly, Birth Defects Res. C. Embryo Today. 81 (2007) 229–240, https://doi.org/10.1002/bdrc.20111.

[44] L.Y. Sakai, D.R. Keene, R.W. Glanville, H.P. Bächinger, Purification and partial characterization of fibrillin, a cysteine-rich structural component of connective tissue microfibrils, J. Biol. Chem. 266 (1991) 14763–14770. http://www.ncbi.nlm.nih.gov/pubmed/1860873.

[45] H.B. Schiller, I.E. Fernandez, G. Burgstaller, C. Schaab, R.A. Scheltema, T. Schwarzmayr, T.M. Strom, O. Eickelberg, M. Mann, Time- and compartment-resolved proteome profiling of the extracellular niche in lung injury and repair, Mol. Syst. Biol. 11 (2015) 819, https://doi.org/10.15252/msb.20156123.

[46] G. Westergren-Thorsson, K. Larsen, K. Nihlberg, A. Andersson-Sjöland, O. Hallgren, G. Marko-Varga, L. Bjermer, Pathological airway remodelling in inflammation, Clin. Res. J. 4 (Suppl 1) (2010) 1–8, https://doi.org/10.1111/j.1752-699X.2010.00190.x.

[47] J.K. Burgess, T. Mauad, G. Tjin, J.C. Karlsson, G. Westergren-Thorsson, The extracellular matrix – the under-recognized element in lung disease? J. Pathol. 240 (2016) 397–409, https://doi.org/10.1002/path.4808.

[48] A. Naba, K.R. Clauser, S. Hoersch, H. Liu, S.A. Carr, R.O. Hynes, The matrisome: in silico definition and in vivo characterization by proteomics of normal and tumor extracellular matrices, Mol. Cell. Proteomics 11 (2012), https://doi.org/10.1074/mcp.M111.014647. M111.014647.

[49] E.S. White, R.G. Atrasz, B. Hu, S.H. Phan, V. Stambolic, T.W. Mak, C. M. Hogaboam, K.R. Flaherty, F.J. Martinez, C.D. Kontos, G.B. Toews, Negative regulation of myofibroblast differentiation by PTEN (phosphatase and tensin homolog deleted on chromosome 10), Am. J. Respir. Crit. Care Med. 173 (2006) 112–121, https://doi.org/10.1164/rccm.200507-1058OC.

[50] U. Hersel, C. Dahmen, H. Kessler, RGD modified polymers: biomaterials for stimulated cell adhesion and beyond, Biomaterials 24 (2003) 4385–4415, https://doi.org/10.1016/S0142-9612(03)00343-0.

[51] M.L. Bedell, A.J. Melchiorri, J. Aleman, A. Skardal, A.G. Mikos, A high-throughput approach to compare the biocompatibility of candidate bioink formulations, Bioprinting 17 (2020), e00068, https://doi.org/10.1016/j.bprint.2019.e00068.

[52] D. Williams, P. Thayer, H. Martinez, E. Gatenholm, A. Khademhosseini, A perspective on the physical, mechanical and biological specifications of bioinks and the development of functional tissues in 3D bioprinting, Bioprinting 9 (2018) 19–36, https://doi.org/10.1016/j.bprint.2018.02.003.

[53] D.F. Williams, On the mechanisms of biocompatibility, Biomaterials 29 (2008) 2941–2953, https://doi.org/10.1016/j.biomaterials.2008.04.023.

[54] K. Dubbin, A. Tabet, S.C. Heilshorn, Quantitative criteria to benchmark new and existing bio-inks for cell compatibility, Biofabrication 9 (2017), https://doi.org/10.1088/1758-5090/aa869f.

[55] J.M. Anderson, A. Rodriguez, D.T. Chang, Foreign body reaction to biomaterials, Semin. Immunol. 20 (2008) 86–100, https://doi.org/10.1016/j.smim.2007.11.004.

[56] D. Yang, K.S. Jones, Effect of alginate on innate immune activation of macrophages, J. Biomed. Mater. Res. A. 90 (2009) 411–418, https://doi.org/10.1002/jbm.a.32096.

[57] G.A. Paredes Juárez, M. Spasojevic, M.M. Faas, P. de Vos, Immunological and technical considerations in application of alginate-based microencapsulation systems, Front. Bioeng. Biotechnol. 2 (2014) 26, https://doi.org/10.3389/fbioe.2014.00026.

[58] S. Rodriguez, R. Tuli, A. Wheeler, A. Nguyen, J. Luong, R. Mohammadi, M. Alexander, J.R.T. Lakey, Current perspective and advancements of alginate-based transplantation technologies, in: Alginates - Recent Uses This Nat. Polym., 2020, https://doi.org/10.5772/intechopen.87120. IntechOpen.

[59] H. Joo, J. Park, C. Sutthiwanjampa, H. Kim, T. Bae, W. Kim, J. Choi, M. Kim, S. Kang, H. Park, Surface coating with hyaluronic acid-gelatin-crosslinked hydrogel on gelatin-conjugated poly(dimethylsiloxane) for implantable medical device-induced fibrosis, Pharmaceutics 13 (2021), https://doi.org/10.3390/pharmaceutics13020269.

[60] J.-T. Kim, D.Y. Lee, E.-J. Kim, J.-W. Jang, N.-I. Cho, Tissue response to implants of hyaluronic acid hydrogel prepared by microbeads, Tissue Eng, Regen. Med. 11 (2014) 32–38, https://doi.org/10.1007/s13770-013-1106-9.

[61] P. Johnson, A.A. Arif, S.S.M. Lee-Sayer, Y. Dong, Hyaluronan and its interactions with immune cells in the healthy and inflamed lung, Front. Immunol. 9 (2018) 2787, https://doi.org/10.3389/fimmu.2018.02787.

[62] Q. Yang, S.K. Lai, Anti-PEG immunity: emergence, characteristics, and unaddressed questions., Wiley Interdiscip. Rev. Nanomed. Nanobiotechnol. 7 (n. d.) 655–77.https://doi.org/10.1002/wnan.1339.

[63] T. Shimizu, Y. Ishima, T. Ishida, Induction of anti-PEG immune responses by PEGylation of proteins, Yakugaku Zasshi 140 (2020) 163–169, https://doi.org/10.1248/yakushi.19-00187-5.

[64] L. Jia, P. Zhang, Z. Ci, W. Zhang, Y. Liu, H. Jiang, G. Zhou, Immune-inflammatory responses of an acellular cartilage matrix biomimetic scaffold in a xenotransplantation goat model for cartilage tissue engineering, Front. Bioeng. Biotechnol. 9 (2021), 667161, https://doi.org/10.3389/fbioe.2021.667161.

[65] M. Huber-Lang, J.D. Lambris, P.A. Ward, Innate immune responses to trauma, Nat. Immunol. 19 (2018) 327–341, https://doi.org/10.1038/s41590-018-0064-8.

[66] R.C. Mettelman, E.K. Allen, P.G. Thomas, Mucosal immune responses to infection and vaccination in the respiratory tract, Immunity 55 (2022) 749–780, https://doi.org/10.1016/j.immuni.2022.04.013.

[67] H. Aegerter, B.N. Lambrecht, C.V. Jakubzick, Biology of lung macrophages in health and disease, Immunity 55 (2022) 1564–1580, https://doi.org/10.1016/j.immuni.2022.08.010.

[68] M.J. Page, D.B. Kell, E. Pretorius, The Role of Lipopolysaccharide-Induced Cell Signalling in Chronic Inflammation., Chronic Stress (Thousand Oaks, Calif.). 6 (n. d.) 24705470221076390 https://doi.org/10.1177/24705470221076390.

[69] M. Hospodiuk, M. Dey, D. Sosnoski, I.T. Ozbolat, The bioink: a comprehensive review on bioprintable materials, Biotechnol. Adv. 35 (2017) 217–239, https://doi.org/10.1016/j.biotechadv.2016.12.006.

[70] D. Chimene, K.K. Lennox, R.R. Kaunas, A.K. Gaharwar, Advanced bioinks for 3D printing: a materials science perspective, Ann. Biomed. Eng. 44 (2016) 2090–2102, https://doi.org/10.1007/s10439-016-1638-y.

[71] G. Gillispie, P. Prim, J. Copus, J. Fisher, A.G. Mikos, J.J. Yoo, A. Atala, S.J. Lee, Assessment methodologies for extrusion-based bioink printability, Biofabrication 12 (2020), 022003, https://doi.org/10.1088/1758-5090/ab6f0d.

[72] S.C. Lee, G. Gillispie, P. Prim, S.J. Lee, Physical and chemical factors influencing the printability of hydrogel-based extrusion bioinks, Chem. Rev. 120 (2020) 10834–10886, https://doi.org/10.1021/acs.chemrev.0c00015.

[73] A. Schwab, R. Levato, M. D'Este, S. Piluso, D. Eglin, J. Malda, Printability and shape fidelity of bioinks in 3D bioprinting, Chem. Rev. 120 (2020) 11028–11055, https://doi.org/10.1021/acs.chemrev.0c00084.

[74] S. Kyle, Z.M. Jessop, A. Al-Sabah, I.S. Whitaker, Printability" of candidate biomaterials for extrusion based 3D printing: state-of-the-art, Adv. Healthc. Mater. 6 (2017), https://doi.org/10.1002/adhm.201700264.

[75] Y. Osada, K. Kajiwara, T. Fushimi, O. Irasa, Y. Hirokawa, T. Matsunaga, T. Shimomura, L. Wang, H. Ishida, Contributors, in: Gels Handb, Elsevier, 2001, https://doi.org/10.1016/B978-012394690-4/50074-8 xxiii–xxx.

[76] L.A. Estroff, A.D. Hamilton, Water gelation by small organic molecules, Chem. Rev. 104 (2004) 1201–1217, https://doi.org/10.1021/cr0302049.

[77] H.J. Van Der Linden, S. Herber, W. Olthuis, P. Bergveld, Stimulus-sensitive hydrogels and their applications in chemical (micro)analysis, Analyst 128 (2003) 325–331, https://doi.org/10.1039/b210140h.

[78] J.L. Drury, D.J. Mooney, Hydrogels for tissue engineering: scaffold design variables and applications, Biomaterials 24 (2003) 4337–4351, https://doi.org/10.1016/S0142-9612(03)00340-5.
[79] K.Y. Lee, D.J. Mooney, Hydrogels for tissue engineering, Chem. Rev. 101 (2001) 1869–1879, https://doi.org/10.1021/cr000108x.
[80] F. Ganji, S. Vasheghani-Farahani, E. Vasheghani-Farahani, Iran, in: J. Polym, English (Eds.), Theoretical Description of Hydrogel Swelling: A Review, vol. 19, 2010, pp. 375–398, http://journal.ippi.ac.ir/journals.php?tab=1&v=19&n=5.
[81] S.C. Owen, M.S. Shoichet, Design of three-dimensional biomimetic scaffolds, J. Biomed. Mater. Res., Part A 94 (2010) 1321–1331, https://doi.org/10.1002/jbm.a.32834.
[82] N. Ashammakhi, S. Ahadian, C. Xu, H. Montazerian, H. Ko, R. Nasiri, N. Barros, A. Khademhosseini, Bioinks and bioprinting technologies to make heterogeneous and biomimetic tissue constructs, Mater. Today Bio. 1 (2019), https://doi.org/10.1016/j.mtbio.2019.100008.
[83] R.S.H. Wong, M. Ashton, K. Dodou, Effect of crosslinking agent concentration on the properties of unmedicated hydrogels, Pharmaceutics 7 (2015) 305–319, https://doi.org/10.3390/pharmaceutics7030305.
[84] J. Maitra, V.K. Shukla, Cross-linking in hydrogels - a review, Am. J. Polym. Sci. 4 (2014) 25–31, https://doi.org/10.5923/j.ajps.20140402.01.
[85] D.E. Discher, P. Janmey, Y.-L. Wang, Tissue cells feel and respond to the stiffness of their substrate, Science 310 (2005) 1139–1143, https://doi.org/10.1126/science.1116995.
[86] E. Hadjipanayi, V. Mudera, R.A. Brown, Close dependence of fibroblast proliferation on collagen scaffold matrix stiffness, J. Tissue Eng. Regen. Med. 3 (2009) 77–84, https://doi.org/10.1002/term.136.
[87] A.Y. Gamal, N.N. Al-Berry, A.A. Hassan, L.A. Rashed, V.J. Iacono, In vitro evaluation of the human gingival fibroblast/gingival mesenchymal stem cell dynamics through perforated guided tissue membranes: cell migration, proliferation and membrane stiffness assay, J. Periodontal. Res. 52 (2017) 628–635, https://doi.org/10.1111/jre.12431.
[88] B. Dessane, R. Smirani, G. Bouguéon, T. Kauss, E. Ribot, R. Devillard, P. Barthélémy, A. Naveau, S. Crauste-Manciet, Nucleotide lipid-based hydrogel as a new biomaterial ink for biofabrication, Sci. Rep. 10 (2020) 2850, https://doi.org/10.1038/s41598-020-59632-w.
[89] K. Dubbin, Y. Hori, K.K. Lewis, S.C. Heilshorn, Dual-stage crosslinking of a gel-phase bioink improves cell viability and homogeneity for 3D bioprinting, Adv. Healthc. Mater. 5 (2016) 2488–2492, https://doi.org/10.1002/adhm.201600636.
[90] K. Schacht, T. Jüngst, M. Schweinlin, A. Ewald, J. Groll, T. Scheibel, Biofabrication of cell-loaded 3D spider silk constructs, Angew. Chem., Int. Ed. Engl. 54 (2015) 2816–2820, https://doi.org/10.1002/anie.201409846.
[91] T.Y. Lee, T.M. Roper, E.S. Jonsson, I. Kudyakov, K. Viswanathan, C. Nason, C. A. Guymon, C.E. Hoyle, The kinetics of vinyl acrylate photopolymerization, Polymer 44 (2003) 2859–2865, https://doi.org/10.1016/S0032-3861(03)00213-1.
[92] V.L. Tsang, A.A. Chen, L.M. Cho, K.D. Jadin, R.L. Sah, S. DeLong, J.L. West, S. N. Bhatia, Fabrication of 3D hepatic tissues by additive photopatterning of cellular hydrogels, Faseb. J. 21 (2007) 790–801, https://doi.org/10.1096/fj.06-7117com.
[93] P. Zorlutuna, N. Annabi, G. Camci-Unal, M. Nikkhah, J.M. Cha, J.W. Nichol, A. Manbachi, H. Bae, S. Chen, A. Khademhosseini, Microfabricated biomaterials for engineering 3D tissues, Adv. Mater. 24 (2012) 1782–1804, https://doi.org/10.1002/adma.201104631.
[94] A.V. Do, B. Khorsand, S.M. Geary, A.K. Salem, 3D printing of scaffolds for tissue regeneration applications, Adv. Healthc. Mater. 4 (2015) 1742–1762, https://doi.org/10.1002/adhm.201500168.
[95] D.A. Banyard, V. Borad, E. Amezcua, G.A. Wirth, G.R.D. Evans, A.D. Widgerow, Preparation, characterization, and clinical implications of human decellularized adipose tissue extracellular matrix (hDAM): a comprehensive review, Aesthetic Surg. J. 36 (2016) 349–357, https://doi.org/10.1093/asj/sjv170.
[96] F. Pati, J. Jang, D.H. Ha, S. Won Kim, J.W. Rhie, J.H. Shim, D.H. Kim, D.W. Cho, Printing three-dimensional tissue analogues with decellularized extracellular matrix bioink, Nat. Commun. 5 (2014) 1–11, https://doi.org/10.1038/ncomms4935.
[97] O. Rosmark, E. Åhrman, C. Müller, L. Elowsson Rendin, L. Eriksson, A. Malmström, O. Hallgren, A.K. Larsson-Callerfelt, G. Westergren-Thorsson, J. Malmström, Quantifying extracellular matrix turnover in human lung scaffold cultures, Sci. Rep. 8 (2018) 1–13, https://doi.org/10.1038/s41598-018-23702-x.
[98] R.H.J. De Hilster, P.K. Sharma, M.R. Jonker, E.S. White, E.A. Gercama, M. Roobeek, W. Timens, M.C. Harmsen, M.N. Hylkema, J.K. Burgess, Human lung extracellular matrix hydrogels resemble the stiffness and viscoelasticity of native lung tissue, Am. J. Physiol. Lung Cell Mol. Physiol. 318 (2020) L698–L704, https://doi.org/10.1152/AJPLUNG.00451.2019.
[99] R.A. Pouliot, P.A. Link, N.S. Mikhaiel, M.B. Schneck, M.S. Valentine, F.J. Kamga Gninzeko, J.A. Herbert, M. Sakagami, R.L. Heise, Development and characterization of a naturally derived lung extracellular matrix hydrogel, J. Biomed. Mater. Res. A. 104 (2016), https://doi.org/10.1002/jbm.a.35726, 1922–35.
[100] J.Y. Park, H. Ryu, B. Lee, D.-H. Ha, M. Ahn, S. Kim, J.Y. Kim, N.L. Jeon, D.-W. Cho, Development of a functional airway-on-a-chip by 3D cell printing, Biofabrication 11 (2018), 015002, https://doi.org/10.1088/1758-5090/aae545.
[101] B. Falcones, H. Sanz-Fraile, E. Marhuenda, I. Mendizábal, I. Cabrera-Aguilera, N. Malandain, J.J. Uriarte, I. Almendros, D. Navajas, D.J. Weiss, R. Farré, J. Otero, Bioprintable lung extracellular matrix hydrogel scaffolds for 3d culture of mesenchymal stromal cells, Polymers 13 (2021) 1–18, https://doi.org/10.3390/polym13142350.
[102] S. Fang, S. Zhang, H. Dai, X. Hu, C. Li, Y. Xing, The role of pulmonary mesenchymal cells in airway epithelium regeneration during injury repair, Stem Cell Res. Ther. 10 (2019) 1–12, https://doi.org/10.1186/s13287-019-1452-1.
[103] L. Horvath, Y. Umehara, C. Jud, F. Blank, A. Petri-Fink, B. Rothen-Rutishauser, Engineering an in vitro air-blood barrier by 3D bioprinting, Sci. Rep. 5 (2015), https://doi.org/10.1038/srep07974.
[104] W.L. Ng, T.C. Ayi, Y.-C. Liu, S.L. Sing, W.Y. Yeong, B.-H. Tan, Fabrication and characterization of 3D bioprinted triple-layered human alveolar lung models, Int. J. Bioprinting. 7 (2021) 53–67, https://doi.org/10.18063/ijb.v7i2.332.
[105] J. Berg, T. Hiller, M.S. Kissner, T.H. Qazi, G.N. Duda, A.C. Hocke, S. Hippenstiel, L. Elomaa, M. Weinhart, C. Fahrenson, J. Kurreck, Optimization of cell-laden bioinks for 3D bioprinting and efficient infection with influenza A virus, Sci. Rep. 8 (2018) 1–13, https://doi.org/10.1038/s41598-018-31880-x.
[106] O. Smidsrød, Molecular basis for some physical properties of alginates in the gel state, Faraday Discuss. Chem. Soc. 57 (1974) 263–274, https://doi.org/10.1039/DC9745700263.
[107] J. Berg, Z. Weber, M. Fechler-Bitteti, A.C. Hocke, S. Hippenstiel, L. Elomaa, M. Weinhart, J. Kurreck, Bioprinted multi-cell type lung model for the study of viral inhibitors, Viruses 13 (2021) 1–17, https://doi.org/10.3390/v13081590.
[108] G. Benton, I. Arnaoutova, J. George, H.K. Kleinman, J. Koblinski, Matrigel: from discovery and ECM mimicry to assays and models for cancer research, 79–80, Adv. Drug Deliv. Rev. (2014) 3–18, https://doi.org/10.1016/j.addr.2014.06.005.
[109] E.A. Aisenbrey, W.L. Murphy, Synthetic alternatives to Matrigel, Nat. Rev. Mater. 5 (2020) 539–551, https://doi.org/10.1038/s41578-020-0199-8.
[110] J. Denner, R.R. Tönjes, Infection barriers to successful xenotransplantation focusing on porcine endogenous retroviruses, Clin. Microbiol. Rev. 25 (2012) 318–343, https://doi.org/10.1128/CMR.05011-11.
[111] M.M. De Santis, H.N. Alsafadi, S. Tas, D.A. Bölükbas, S. Prithiviraj, I.A.N. Da Silva, M. Mittendorfer, C. Ota, J. Stegmayr, F. Daoud, M. Königshoff, K. Swärd, J. A. Wood, M. Tassieri, P.E. Bourgine, S. Lindstedt, S. Mohlin, D.E. Wagner, Extracellular-matrix-reinforced bioinks for 3D bioprinting human tissue, Adv. Mater. 33 (2021), https://doi.org/10.1002/adma.202005476.
[112] E. Axpe, M.L. Oyen, Applications of alginate-based bioinks in 3D bioprinting, Int. J. Mol. Sci. 17 (2016), https://doi.org/10.3390/ijms17121976.
[113] G.T. Grant, E.R. Morris, D.A. Rees, P.J.C. Smith, D. Thom, Biological interactions between polysaccharides and divalent cations: the egg-box model, FEBS Lett. 32 (1973) 195–198, https://doi.org/10.1016/0014-5793(73)80770-7.
[114] F. Della Sala, M. di Gennaro, G. Lista, F. Messina, L. Ambrosio, A. Borzacchiello, Effect of hyaluronic acid on the differentiation of mesenchymal stem cells into mature type II pneumocytes, Polymers 13 (2021), https://doi.org/10.3390/polym13172928.
[115] J.A. Burdick, G.D. Prestwich, Hyaluronic acid hydrogels for biomedical applications, Adv. Mater. 23 (2011) 41–56, https://doi.org/10.1002/adma.201003963.
[116] M. Djabourov, J.P. Lechaire, F. Gaill, Structure and rheology of gelatin and collagen gels, Biorheology 30 (1993) 191–205, https://doi.org/10.3233/bir-1993-303-405.
[117] T. Billiet, E. Gevaert, T. De Schryver, M. Cornelissen, P. Dubruel, The 3D printing of gelatin methacrylamide cell-laden tissue-engineered constructs with high cell viability, Biomaterials 35 (2014) 49–62, https://doi.org/10.1016/j.biomaterials.2013.09.078.
[118] W. Schuurman, P.A. Levett, M.W. Pot, P.R. van Weeren, W.J.A. Dhert, D. W. Hutmacher, F.P.W. Melchels, T.J. Klein, J. Malda, Gelatin-methacrylamide hydrogels as potential biomaterials for fabrication of tissue-engineered cartilage constructs, Macromol. Biosci. 13 (2013) 551–561, https://doi.org/10.1002/mabi.201200471.
[119] L.E. Bertassoni, J.C. Cardoso, V. Manoharan, A.L. Cristino, N.S. Bhise, W. A. Araujo, P. Zorlutuna, N.E. Vrana, A.M. Ghaemmaghami, M.R. Dokmeci, A. Khademhosseini, Direct-write bioprinting of cell-laden methacrylated gelatin hydrogels, Biofabrication 6 (2014), 024105, https://doi.org/10.1088/1758-5082/6/2/024105.
[120] E. Hoch, T. Hirth, G.E.M. Tovar, K. Borchers, Chemical tailoring of gelatin to adjust its chemical and physical properties for functional bioprinting, J. Mater. Chem. B. 1 (2013) 5675, https://doi.org/10.1039/c3tb20745e.
[121] T. Asakura, J. Yao, T. Yamane, K. Umemura, A.S. Ulrich, Heterogeneous structure of silk fibers from Bombyx mori resolved by 13C solid-state NMR spectroscopy, J. Am. Chem. Soc. 124 (2002), https://doi.org/10.1021/ja020244e, 8794–5.
[122] R. Nazarov, H.-J. Jin, D.L. Kaplan, Porous 3-D scaffolds from regenerated silk fibroin, Biomacromolecules 5 (2004) 718–726, https://doi.org/10.1021/bm034327e.
[123] U.-J. Kim, J. Park, C. Li, H.-J. Jin, R. Valluzzi, D.L. Kaplan, Structure and properties of silk hydrogels, Biomacromolecules 5 (2004) 786–792, https://doi.org/10.1021/bm0345460.
[124] U.-J. Kim, J. Park, H.J. Kim, M. Wada, D.L. Kaplan, Three-dimensional aqueous-derived biomaterial scaffolds from silk fibroin, Biomaterials 26 (2005) 2775–2785, https://doi.org/10.1016/j.biomaterials.2004.07.044.
[125] L. Huang, W. Yuan, Y. Hong, S. Fan, X. Yao, T. Ren, L. Song, G. Yang, Y. Zhang, 3D Printed Hydrogels with Oxidized Cellulose Nanofibers and Silk Fibroin for the Proliferation of Lung Epithelial Stem Cells, Cellul., London, England), 2020, pp. 1–17, https://doi.org/10.1007/s10570-020-03526-7.
[126] M.S. Ibrahim, N.A. El-Wassefy, D.S. Farahat, Biocompatibility of dental biomaterials, in: Biomater. Oral Dent. Tissue Eng., Elsevier, 2017, pp. 117–140, https://doi.org/10.1016/B978-0-08-100961-1.00008-6.

[127] K.J.R. Lewis, M.W. Tibbitt, Y. Zhao, K. Branchfield, X. Sun, V. Balasubramaniam, K.S. Anseth, In vitro model alveoli from photodegradable microsphere templates, Biomater. Sci. 3 (2015) 821–832, https://doi.org/10.1039/c5bm00034c.

[128] M. Tako, S. Nakamura, Gelation mechanism of agarose, Carbohydr. Res. 180 (1988) 277–284, https://doi.org/10.1016/0008-6215(88)80084-3.

[129] C.T. Buckley, S.D. Thorpe, F.J. O'Brien, A.J. Robinson, D.J. Kelly, The effect of concentration, thermal history and cell seeding density on the initial mechanical properties of agarose hydrogels, J. Mech. Behav. Biomed. Mater. 2 (2009) 512–521, https://doi.org/10.1016/j.jmbbm.2008.12.007.

[130] Y.J. Tan, X. Tan, W.Y. Yeong, S.B. Tor, Hybrid microscaffold-based 3D bioprinting of multi-cellular constructs with high compressive strength: a new biofabrication strategy, Sci. Rep. 6 (2016), 39140, https://doi.org/10.1038/srep39140.

[131] M. Köpf, D.F.D. Campos, A. Blaeser, K.S. Sen, H. Fischer, A tailored three-dimensionally printable agarose-collagen blend allows encapsulation, spreading, and attachment of human umbilical artery smooth muscle cells, Biofabrication 8 (2016) 1–15, https://doi.org/10.1088/1758-5090/8/2/025011.

[132] R. Lozano, L. Stevens, B.C. Thompson, K.J. Gilmore, R. Gorkin, E.M. Stewart, M. in het Panhuis, M. Romero-Ortega, G.G. Wallace, 3D printing of layered brain-like structures using peptide modified gellan gum substrates, Biomaterials 67 (2015) 264–273, https://doi.org/10.1016/j.biomaterials.2015.07.022.

[133] Z. Tan, C. Parisi, L. Di Silvio, D. Dini, A.E. Forte, Cryogenic 3D printing of super soft hydrogels, Sci. Rep. 7 (2017), 16293, https://doi.org/10.1038/s41598-017-16668-9.

[134] M.T. Stubbs, W. Bode, A player of many parts: the spotlight falls on thrombin's structure, Thromb. Res. 69 (1993) 1–58, https://doi.org/10.1016/0049-3848(93)90002-6.

[135] B. Blombäck, B. Hessel, D. Hogg, L. Therkildsen, A two-step fibrinogen–fibrin transition in blood coagulation, Nature 275 (1978) 501–505, https://doi.org/10.1038/275501a0.

[136] M. Nakamura, S. Iwanaga, C. Henmi, K. Arai, Y. Nishiyama, Biomatrices and biomaterials for future developments of bioprinting and biofabrication, Biofabrication 2 (2010), 014110, https://doi.org/10.1088/1758-5082/2/1/014110.

[137] E.M. Ahmed, Hydrogel: preparation, characterization, and applications: a review, J. Adv. Res. 6 (2015), https://doi.org/10.1016/j.jare.2013.07.006.

[138] M.J. Serpe, C.D. Jones, L.A. Lyon, Layer-by-Layer deposition of thermoresponsive microgel thin films, Langmuir 19 (2003), https://doi.org/10.1021/la034391h.

[139] F.A. Plamper, W. Richtering, Functional microgels and microgel systems, Acc. Chem. Res. 50 (2017), https://doi.org/10.1021/acs.accounts.6b00544.

[140] J.A. Bonham, M.A. Faers, J.S. Van Duijneveldt, Non-aqueous microgel particles: synthesis, properties and applications, Soft Matter 10 (2014), https://doi.org/10.1039/c4sm01834f.

[141] A.C. Daly, L. Riley, T. Segura, J.A. Burdick, Hydrogel microparticles for biomedical applications, Nat. Rev. Mater. 5 (2020), https://doi.org/10.1038/s41578-019-0148-6.

[142] H. Staudinger, E. Husemann, Über hochpolymere Verbindungen, 116. Mitteil.: Über das begrenzt quellbare Poly-styrol, Berichte Der Dtsch. Chem. Gesellschaft (A B Ser. 68 (1935), https://doi.org/10.1002/cber.19350680841.

[143] W.O. Baker, Microgel, A new macromolecule, Ind. Eng. Chem. 41 (1949), https://doi.org/10.1021/ie50471a016.

[144] R.H. Pelton, P. Chibante, Preparation of aqueous latices with N-isopropylacrylamide, Colloid. Surface. 20 (1986), https://doi.org/10.1016/0166-6622(86)80274-8.

[145] M. Wei, M.J. Serpe, Temperature–light dual-responsive Au@PNIPAm core-shell microgel-based optical devices, Part. Part. Syst. Char. 36 (2019), https://doi.org/10.1002/ppsc.201800326.

[146] M. Das, S. Mardyani, W.C.W. Chan, E. Kumacheva, Biofunctionalized pH-responsive microgels for cancer cell targeting: rational design, Adv. Mater. 18 (2006), https://doi.org/10.1002/adma.200501043.

[147] Y. Gao, X. Li, M.J. Serpe, Stimuli-responsive microgel-based etalons for optical sensing, RSC Adv. 5 (2015), https://doi.org/10.1039/c5ra02306h.

[148] W. Xu, Y. Zhang, Y. Gao, M.J. Serpe, Electrically triggered small molecule release from poly(N -isopropylacrylamide- co -acrylic acid) microgel-modified electrodes, ACS Appl. Mater. Interfaces 10 (2018), https://doi.org/10.1021/acsami.8b04053.

[149] A. Biffis, N. Orlandi, B. Corain, Microgel-stabilized metal nanoclusters: size control by microgel nanomorphology, Adv. Mater. 15 (2003), https://doi.org/10.1002/adma.200304977.

[150] L.A. Lyon, Z. Meng, N. Singh, C.D. Sorrell, A.S. John, Thermoresponsive microgel-based materials, Chem. Soc. Rev. 38 (2009), https://doi.org/10.1039/b715522k.

[151] M. Chen, L. Zhou, Y. Guan, Y. Zhang, Polymerized microgel colloidal crystals: photonic hydrogels with tunable band gaps and fast response rates, Angew. Chem. Int. Ed. 52 (2013), https://doi.org/10.1002/anie.201302466.

[152] M. Wei, Y. Gao, X. Li, M.J. Serpe, Stimuli-responsive polymers and their applications, Polym. Chem. 8 (2017), https://doi.org/10.1039/c6py01585a.

[153] B.P. Tripathi, N.C. Dubey, M. Stamm, Hollow microgel based ultrathin thermoresponsive membranes for separation, synthesis, and catalytic applications, ACS Appl. Mater. Interfaces 6 (2014), https://doi.org/10.1021/am504120c.

[154] Y. Gao, G.P. Zago, Z. Jia, M.J. Serpe, Controlled and triggered small molecule release from a confined polymer film, ACS Appl. Mater. Interfaces 5 (2013), https://doi.org/10.1021/am4029894.

[155] Y. Gao, A. Ahiabu, M.J. Serpe, Controlled drug release from the aggregation-disaggregation behavior of pH-responsive microgels, ACS Appl. Mater. Interfaces 6 (2014), https://doi.org/10.1021/am503200p.

[156] Y. Gao, K.Y. Wong, A. Ahiabu, M.J. Serpe, Sequential and controlled release of small molecules from poly(: N -isopropylacrylamide) microgel-based reservoir devices, J. Mater. Chem. B. 4 (2016), https://doi.org/10.1039/c6tb00864j.

[157] C.D. Sorrell, M.C.D. Carter, M.J. Serpe, Color tunable poly (N-Isopropylacrylamide)-co-acrylic acid microgel-Au hybrid assemblies, Adv. Funct. Mater. 21 (2011), https://doi.org/10.1002/adfm.201001714.

[158] B. Zhang, S. Sun, P. Wu, Synthesis and unusual volume phase transition behavior of poly(N-isopropylacrylamide)-poly(2-hydroxyethyl methacrylate) interpenetrating polymer network microgel, Soft Matter 9 (2013), https://doi.org/10.1039/c2sm27355a.

[159] N. He, Q. Cao, L. Wang, X. Chen, B. Li, Z. Liu, Carbon dioxide-switchable chitosan/polymer composite nanogels, Macromol. Chem. Phys. 219 (2018), https://doi.org/10.1002/macp.201800319.

[160] S.V. Murphy, P. De Coppi, A. Atala, Opportunities and challenges of translational 3D bioprinting, Nat. Biomed. Eng. 4 (2020), https://doi.org/10.1038/s41551-019-0471-7.

[161] P.S. Gungor-Ozkerim, I. Inci, Y.S. Zhang, A. Khademhosseini, M.R. Dokmeci, Bioinks for 3D bioprinting: an overview, Biomater. Sci. 6 (2018), https://doi.org/10.1039/c7bm00765e.

[162] W. Liu, M.A. Heinrich, Y. Zhou, A. Akpek, N. Hu, X. Liu, X. Guan, Z. Zhong, X. Jin, A. Khademhosseini, Y.S. Zhang, Extrusion bioprinting of shear-thinning gelatin methacryloyl bioinks, Adv. Healthc. Mater. 6 (2017), https://doi.org/10.1002/adhm.201601451.

[163] W. Liu, Y.S. Zhang, M.A. Heinrich, F. De Ferrari, H.L. Jang, S.M. Bakht, M. M. Alvarez, J. Yang, Y.C. Li, G. Trujillo-de Santiago, A.K. Miri, K. Zhu, P. Khoshakhlagh, G. Prakash, H. Cheng, X. Guan, Z. Zhong, J. Ju, G.H. Zhu, X. Jin, S.R. Shin, M.R. Dokmeci, A. Khademhosseini, Rapid continuous multimaterial extrusion bioprinting, Adv. Mater. 29 (2017), https://doi.org/10.1002/adma.201604630.

[164] C.W. Peak, J. Stein, K.A. Gold, A.K. Gaharwar, Nanoengineered colloidal inks for 3D bioprinting, Langmuir 34 (2018), https://doi.org/10.1021/acs.langmuir.7b02540.

[165] N. Law, B. Doney, H. Glover, Y. Qin, Z.M. Aman, T.B. Sercombe, L.J. Liew, R. J. Dilley, B.J. Doyle, Characterisation of hyaluronic acid methylcellulose hydrogels for 3D bioprinting, J. Mech. Behav. Biomed. Mater. 77 (2018), https://doi.org/10.1016/j.jmbbm.2017.09.031.

[166] R. Schwartz, M. Malpica, G.L. Thompson, A.K. Miri, Cell encapsulation in gelatin bioink impairs 3D bioprinting resolution, J. Mech. Behav. Biomed. Mater. 103 (2020), https://doi.org/10.1016/j.jmbbm.2019.103524.

[167] M. Askari, M. Afzali Naniz, M. Kouhi, A. Saberi, A. Zolfagharian, M. Bodaghi, Recent progress in extrusion 3D bioprinting of hydrogel biomaterials for tissue regeneration: a comprehensive review with focus on advanced fabrication techniques, Biomater. Sci. 9 (2021), https://doi.org/10.1039/d0bm00973c.

[168] C. Mandrycky, Z. Wang, K. Kim, D.H. Kim, 3D bioprinting for engineering complex tissues, Biotechnol. Adv. 34 (2016), https://doi.org/10.1016/j.biotechadv.2015.12.011.

[169] I. Matai, G. Kaur, A. Seyedsalehi, A. McClinton, C.T. Laurencin, Progress in 3D bioprinting technology for tissue/organ regenerative engineering, Biomaterials 226 (2020), https://doi.org/10.1016/j.biomaterials.2019.119536.

[170] D. Chester, P. Theetharappan, T. Ngobili, M. Daniele, A.C. Brown, Ultrasonic microplotting of microgel bioinks, ACS Appl. Mater. Interfaces 12 (2020) 47309–47319, https://doi.org/10.1021/acsami.0c15056.

[171] D. Chester, P. Theetharappan, T. Ngobili, M. Daniele, A.C. Brown, Ultrasonic microplotting of microgel bioinks, ACS Appl. Mater. Interfaces 12 (2020), https://doi.org/10.1021/acsami.0c15056.

[172] C.B. Highley, K.H. Song, A.C. Daly, J.A. Burdick, Jammed microgel inks for 3D printing applications, Adv. Sci. 6 (2019), https://doi.org/10.1002/advs.201801076.

[173] Y. Zhang, S.T. Ellison, S. Duraivel, C.D. Morley, C.R. Taylor, T.E. Angelini, 3D printed collagen structures at low concentrations supported by jammed microgels, Bioprinting 21 (2021), https://doi.org/10.1016/j.bprint.2020.e00121.

[174] S. Xin, D. Chimene, J.E. Garza, A.K. Gaharwar, D.L. Alge, Clickable PEG hydrogel microspheres as building blocks for 3D bioprinting, Biomater. Sci. 7 (2019), https://doi.org/10.1039/c8bm01286e.

[175] O. Jeon, Y.B. Lee, T.J. Hinton, A.W. Feinberg, E. Alsberg, Cryopreserved cell-laden alginate microgel bioink for 3D bioprinting of living tissues, Mater. Today Chem. 12 (2019), https://doi.org/10.1016/j.mtchem.2018.11.009.

[176] J.-M. Lehn, Toward complex matter: supramolecular chemistry and self-organization, Proc. Natl. Acad. Sci. U. S. A 99 (2002) 4763–4768, https://doi.org/10.1073/pnas.072065599.

[177] W. Han, W. Xiang, Q. Li, H. Zhang, Y. Yang, J. Shi, Y. Ji, S. Wang, X. Ji, N. M. Khashab, J.L. Sessler, Water compatible supramolecular polymers: recent progress, Chem. Soc. Rev. 50 (2021) 10025–10043, https://doi.org/10.1039/d1cs00187f.

[178] P.R.A. Chivers, D.K. Smith, Spatially-resolved soft materials for controlled release - hybrid hydrogels combining a robust photo-activated polymer gel with an interactive supramolecular gel, Chem. Sci. 8 (2017) 7218–7227, https://doi.org/10.1039/c7sc02210g.

[179] A. Biswas, S. Malferrari, D.M. Kalaskar, A.K. Das, Arylboronate esters mediated self-healable and biocompatible dynamic G-quadruplex hydrogels as promising 3D-bioinks, Chem. Commun. 54 (2018) 1778–1781, https://doi.org/10.1039/C7CC09051J.

[180] B. Dessane, R. Smirani, G. Bouguéon, T. Kauss, E. Ribot, R. Devillard, P. Barthélémy, A. Naveau, S. Crauste-Manciet, Nucleotide lipid-based hydrogel as a new biomaterial ink for biofabrication, Sci. Rep. 10 (2020) 1–11, https://doi.org/10.1038/s41598-020-59632-w.

[181] H. Shigemitsu, I. Hamachi, Design strategies of stimuli-responsive supramolecular hydrogels relying on structural analyses and cell-mimicking approaches, Acc. Chem. Res. 50 (2017) 740–750, https://doi.org/10.1021/acs.accounts.7b00070.
[182] R. Laishram, S. Sarkar, I. Seth, N. Khatun, V.K. Aswal, U. Maitra, S.J. George, Secondary nucleation-triggered physical cross-links and tunable stiffness in seeded supramolecular hydrogels, J. Am. Chem. Soc. 144 (2022) 11306–11315, https://doi.org/10.1021/jacs.2c03230.
[183] P.R.A. Chivers, D.K. Smith, Shaping and structuring supramolecular gels, Nat. Rev. Mater. 4 (2019) 463–478, https://doi.org/10.1038/s41578-019-0111-6.
[184] M.C. Nolan, A.M. Fuentes Caparrós, B. Dietrich, M. Barrow, E.R. Cross, M. Bleuel, S.M. King, D.J. Adams, Optimising low molecular weight hydrogels for automated 3D printing, Soft Matter 13 (2017) 8426–8432, https://doi.org/10.1039/C7SM01694H.
[185] L.A.J. Rutgeerts, A.H. Soultan, R. Subramani, B. Toprakhisar, H. Ramon, M. C. Paderes, W.M. De Borggraeve, J. Patterson, Robust scalable synthesis of a bis-urea derivative forming thixotropic and cytocompatible supramolecular hydrogels, Chem. Commun. 55 (2019) 7323–7326, https://doi.org/10.1039/C9CC02927C.
[186] P.S. Sheet, D. Koley, Dendritic hydrogel bioink for 3D printing of bacterial microhabitat, ACS Appl. Bio Mater. 2 (2019) 5941–5948, https://doi.org/10.1021/acsabm.9b00866.
[187] A. Chalard, M. Mauduit, S. Souleille, P. Joseph, L. Malaquin, J. Fitremann, 3D printing of a biocompatible low molecular weight supramolecular hydrogel by dimethylsulfoxide water solvent exchange, Addit. Manuf. 33 (2020), 101162, https://doi.org/10.1016/j.addma.2020.101162.